DRFC/CAD FR9601630 EUR-CEA-FC-1520

Conceptual Study of a Reflector Waveguide Array for Launching Lower Hybrid Waves in Reactor-Grade Plasmas

Ph. BIBET, X. LITAUDON, D. MOREAU

Septembre 1994

CEA EURATOM

ASSOCIATION EURATOM-C.E.A.
DEPARTEMENT DE RECHERCHES SUR LA FUSION CONTROLEE
C.E.N./CADARACHE
13108 SAINT PAUL LEZ DURANCE CEDEX

Conceptual Study of a Reflector Array for Launching Lower Hybrid Waves in Reactor-Grade Plasmas

Ph. Bibet, X. Litaudon, D. Moreau
Département de Recherches sur la Fusion Contrôlée
Association EURATOM-CEA
Centre d'Etudes de Cadarache
13108 St Paul lez Durance Cedex, France

Submitted for publication in Nuclear Fusion

CONCEPTUAL STUDY OF A REFLECTOR ARRAY FOR LAUNCHING LOWER HYBRID WAVES IN REACTOR-GRADE PLASMAS

Ph. Bibet, X. Litaudon, D. Moreau

Département de Recherches sur la Fusion Contrôlée
Association Euratom-CEA
Centre d'Etudes de Cadarache
13108 St Paul lez Durance Cedex, France

ABSTRACT

A new concept - the reflector waveguide array - is proposed to improve and simplify the design of c.w. Lower Hybrid launchers for steady-state reactor applications. Mechanical robustness of the antenna and efficient heat removal are provided by a thick-wall waveguide structure which can accomodate a large number of cooling ducts. The plasma facing mouthpiece could be made of the same material as the reactor first wall and could be easily replaceable through remote handling. In order to compensate for the increased horizontal distance between adjacent waveguides, the front ends of the thick septa are grooved to form short ($\approx \lambda/4$) passive waveguides which act as reflectors between the r.f.-powered waveguides (drivers). Then, for an adequate phasing between the active waveguides, the total electric field at the reflector waveguide apertures varies coherently with the one in the drivers to launch a highly directional slow wave. It is shown that the coupling properties of such an array and the directivity of the radiated power spectrum are similar to the ones of present day launchers. Their dependences upon the depth of the reflector waveguides, and the electron density and its gradient are investigated. The effect of changing the phase between the drivers is also studied. The proposed reflector LH antenna would provide enough flexibility to vary the $N_{//}$ spectrum for plasma control purposes in a steady-state fusion reactor.

1. INTRODUCTION

Recent progress in obtaining enhanced plasma confinement and stability, in particular through the modifications of the current density profile, has led to a new reactor concept - the so-called "Advanced Tokamak" concept - which appears promising and economical, with a significant relaxation on the plasma current constraint and the potential for steady-state operation. In such high-bootstrap-component ($\approx$ 60-70%) plasmas, the additional current drive necessary for non-inductive operation and the required feedback control of the total current density profile could be most efficiently obtained with a combination of Lower Hybrid Current Drive (LHCD) together with a seed current in the plasma centre generated - if necessary - by Fast Wave Current Drive (FWCD).

Multi-megawatts Lower Hybrid (LH) launchers are presently made of large waveguide arrays. Considering that the power density in the waveguides can reach 50 MW/m^2 for a

frequency around 5 GHz, and that the necessary injected power would be of the order of 50 to 100 MW for continuous reactor operation, the total number of waveguides composing the antennas would be several thousands [1]. Present concepts in which these waveguides need to be very closely packed do not offer much cooling space and mechanical strength. Therefore, in order to extrapolate the reliable techniques of phased waveguide arrays to a steady-state reactor environment, it would be highly desirable to develop advanced launcher concepts which should be both simpler and more robust, and should allow for efficient heat removal so as to withstand large thermal power loads and mechanical stresses.

A number of studies have already been carried out or are underway in the aim of simplifying the power transmission in the vacuum part of the LH launchers which lies between the RF vacuum windows and the proper coupling structure of the antenna which approaches the plasma scrape-off layer. Among such proposals are the hyperguide concept [2], the use of toroidal oversized waveguides [3] and of poloidal mode converters [4].

As far as the plasma facing component is concerned, new ideas involve the use of wave diffraction through vertical rod arrays to excite a slow travelling wave in the plasma [5-6]. The concept of a so-called quasi-optical grill thus emerged and small antennas based on this concept are presently under design for the purpose of being tested on existing Tokamaks. However this concept suffers intrinsically from a weak plasma coupling for a single pass of the wave through the array because the main wave component excited by the diffracting array does not propagate in the plasma. Acceptable coupling efficiencies can be obtained in principle due to multiple passes of the wave propagating through a resonant double rod array over a sufficient toroidal extension, but this remains to be demonstrated in an experiment.

In this paper, another concept - the reflector waveguide array - is proposed to improve and simplify the design of c.w. LH launchers for steady-state reactor applications [7]. The mechanical robustness of the antenna and an efficient heat removal are provided by a thick-wall waveguide structure which can accomodate a large number of cooling ducts and offers at the same time an appreciable neutron shielding. It therefore allows the use of high poloidally oversized waveguides and thus a large reduction in the total number of waveguides. The plasma facing mouthpiece called a reflector array could be made of the same material as the reactor first wall and could be easily replaceable through remote handling.

After a general description of the guiding principles which led to this new concept, it will be shown that the coupling efficiency of such an array and the directivity of the radiated power spectrum are very similar to the ones of present day launchers.

2. PRINCIPLE OF THE LOWER HYBRID REFLECTOR WAVEGUIDE ARRAY

The basic principle of a slow wave launcher in the LH frequency range is to provide an oscillating electric field which is polarized along the d.c. equilibrium magnetic field and has a wavelength along this field short enough to excite a slow wave which can propagate in the

plasma, i.e. whose refraction index in the direction parallel to the magnetic field is larger than unity ($N_{//} > 1$). Thus present-day LH antennas (grills) are made by a close juxtaposition of narrow waveguides, all powered with the proper phase so that the radiated $N_{//}$-power spectrum peaks at the desired value for good penetration of the waves and efficient current drive. However, for reactor applications in which the waveguides should be poloidally oversized in order to reduce their number by a large factor, this close packing of oversized waveguides would not leave much space for cooling, neutron shielding, and for providing the required mechanical strength to the resulting launching structure in the event of plasma disruptions. A thick-wall waveguide array would therefore offer potential advantages in all these respects. In order to compensate for the increased horizontal distance between adjacent waveguides and still excite the desired $N_{//}$-power spectrum, the front ends of the thick septa could be grooved to form short ($\approx \lambda/4$) passive waveguides which act as reflectors between the r.f.-powered waveguides (Fig. 1). For an adequate phasing between the active waveguides - "drivers" in reflector antenna terminology - the total electric field at the reflector waveguide apertures would then vary coherently with the one in the drivers to launch a highly directional slow wave.

For the purpose of the following calculations, we shall assume that the waveguides (vertical parallel plates) and the plasma are infinitely high. Let 2φ be the phase shift between the active (driver) waveguides, l_{cc} the depth of the passive (reflector) ones and 2Δ the horizontal distance between two consecutive active waveguides of the array. The total electric field E at the aperture of the passive waveguides, i.e. at the interface between the plasma and the antenna, is given by the following approximate relation :

$$E = S_{12}\, e^{j\varphi}\, 2\cos\varphi \left(1 - e^{-j\frac{4\pi\, l_{cc}}{\lambda}}\right) \qquad (1)$$

where S_{12} is the cross coupling parameter through the plasma between active and passive waveguides, and λ is the vacuum wavelength. Therefore to obtain the best coherence in amplitude and phase between drivers and reflectors, for a given frequency, the optimum depth of the passive waveguide should be a compromise in order to simultaneously :

i) maximize the amplitude of the total electric field at the aperture of the passive waveguides (this is obtained for a passive waveguide depth $l_{cc} \approx \lambda/4$) ;

ii) adjust the phase shift between active and passive waveguides to be close to φ.

The optimum depth of the passive waveguides thus depends upon the cross-coupling parameters S_{12} and therefore must be studied as a function of the electron density, n_e, the electron density gradient, ∇n_e, and the geometric periodicity, Δ, of the array.

Assuming that the active waveguides are independently powered, and neglecting the effect of the reflector waveguides, the positions of the successive peaks $N_{//n}$ of the radiated spectrum are given by :

$$N_{//n} = \frac{\varphi}{k\Delta} + n\frac{\pi}{k\Delta} \qquad (2)$$

where k is the vacuum wavenumber. Therefore the choice of the main peak of the radiated $N_{//}$ spectrum ($N_{//0}$, generally around 2) will define the geometry and phasing of the array. For example, if the phase is chosen to be $2\pi/3$ and if the selected $N_{//}$ peak value is 2 for n=0, then $k\Delta = \pi/3$ or $\Delta = \lambda/6$. However, the relation (2) gives $N_{//n} = 2 + 3n$ which shows that a parasitic peak in the $N_{//}$ spectrum appears at $N_{//} = -1$ for $n = -1$. Part of this peak would be in the zone $|N_{//}| < 1$ leading to a strong reflection from the plasma. Also, without the beneficial effect of the reflector waveguides, the successive peaks in the spectrum would be 2 times as close as for a classical antenna in which all waveguides are active and independently powered.

The use of passive waveguides, thanks to the amplitude and phase coherence of the total electric field excited at the waveguide apertures, allows to significantly reduce the height of all odd order peaks, thus strongly attenuating the $n = -1$ one and improving the wave coupling.

To prove that such a concept can be used for the design of a reactor LH launcher, the coupling properties and the $N_{//}$ radiated spectrum have been studied as a function of both :

- plasma parameters, namely, the electron density n_e and electron density gradient ∇n_e ,
- antenna parameters, namely, the passive waveguide depth (l_{cc}), the phase shift between driver waveguides (2φ), the toroidal geometric periodicity (Δ), and the thickness of the septa separating the waveguides in the mouthpiece (e).

3. COUPLING PROPERTIES OF THE REFLECTOR WAVEGUIDE ARRAY

The following computations have been done using the SWAN code [8-9] which has been validated by many comparisons with experiments [10]. An array of 19 waveguides has been considered with 10 passive waveguides juxtaposed in alternance with 9 active ones which have been supposed to be independently powered. The chosen frequency is 5 GHz, and, to satisfy the boundary conditions at the antenna-plasma interface, two evanescent higher modes have been retained in addition to the main fundamental propagating mode.

Two different cases for the geometric periodicity and phase shift have been studied giving the same value of $N_{//0} \approx 2$, the first one with a periodicity of 10 mm and a phase shift $\varphi = 120$ degrees, and the other one with a periodicity of 11.25 mm and a phase shift $\varphi = 135$ degrees. In the first case $2\pi/3$ multijunctions can be used for which the resulting reflection coefficient scales as ρ^3 (ρ being the reflection coefficient at the plasma-antenna interface) and in the second one $\pi/2$ multijunctions can be used for which the reflection coefficient scales as ρ^2 [8-9].

3.1. Dependence of the results on the electron density

When the electron density changes, the main parameter which varies in the problem is the cross-coupling coefficient between adjacent waveguides through the plasma. Its

amplitude decreases when the plasma density increases, as seen on fig. 2 where the electron density gradient has been kept constant (7.3 x 10^{11} cm^{-4}) and the passive waveguides depth is 12 mm.

The two principal output parameters which have been studied are the mean reflection coefficient in the active waveguides and the power directivity.

i) On fig. 3 it appears that in the two cases of different geometric periodicities the mean reflection coefficient in the active waveguides, R, has a minimum at around 3 times the electron cutoff density, n_{ec}, which is 3.1 x 10^{11} cm^{-3} at the chosen frequency. The main difference from more classical antennas is that at the electron cutoff density the reflection coefficient is much lower than 100 % due to the change of the plasma surface admittance. That is explained by a change of the cross-coupling coefficient and also by the fact that the active waveguides are far from each other which allows better radiating properties in vacuum.

ii) For the power directivity, η_p, which is defined by :

$$\eta_p = \int_1^{\infty} \frac{dP}{dN_{//}} dN_{//} \Big/ \int_{-\infty}^{\infty} \frac{dP}{dN_{//}} dN_{//} \qquad (3)$$

and for the $N_{//}$-weighted directivity, η_{cd}, which is defined with respect to current drive efficiency [9] and given by :

$$\eta_{cd} = (1 - R) N_{//\,peak}^2 \left(\int_1^{\infty} \frac{1}{N_{//}^2} \frac{dP}{dN_{//}} dN_{//} - \int_{-\infty}^{-1} \frac{1}{N_{//}^2} \frac{dP}{dN_{//}} dN_{//} \right) \qquad (4)$$

the decrease is quite slow (fig. 4). Near the cutoff electron density the power directivity is around 70 %. The difference in the $N_{//}$-weighted directivity (defined for $N_{//peak} = 2$) for the two periodicities is due to the presence of a peak in the radiated spectrum near $N_{//} = -1$ for the case l_{cc} = 10 mm, corresponding to the order n = -1.

3.2.Dependence of the results on the electron density gradient

For a given electron density of twice the electron cutoff density the chosen variation of the density gradient is corresponding to a change of the electron decay length from 5 to 20 mm. Here, as in the previous paragraph, the main influence of the density gradient variation is on the cross-coupling parameter, S_{12}, which amplitude increases when the gradient of the density is higher (fig. 5). This leads to an improvement of the coupling properties shown on fig. 6. The values corresponding to the case with a geometric periodicity of 11.25 mm are a little higher due to the choice of the passive waveguide depth l_{cc} = 12 mm. The effect on the antenna directivity is quite small (fig 7).

3.3.Dependence of the results on the reflector waveguide depth

As shown in (1) the depth l_{cc} will influence the value of the total electric field at the plasma antenna interface. The optimum value for a given cross-coupling coefficient (S_{12}) and a given phase shift between active waveguides (2φ) is a compromise between a maximization of the total electric field amplitude at the reflector waveguide apertures and the coherent shift of its phase with the phase in the neighbouring active driver. In fig. 8 the mean reflection coefficient of the complete array shows a minimum which is lower for the case Δ = 11.25 mm. This is due to the cancellation of the peak in the radiated spectrum corresponding to the order n = -1, and occurs with a phase shift $2\varphi = 270°$. As anticipated before, the resulting optimum depth is close to $\lambda/4$ = 15 mm.

The influence on the power directivity and $N_{//}$-weighted directivity ($N_{//peak} = 2$) is shown in fig. 9. The maximum directivity occurs nearly for the same optimum value of l_{cc} , i.e. the one which leads to the best coupling properties. A variation of the order of 2 to 3 mm ($\approx$ 20 %) of the depth can be allowed around the optimum value, and therefore the choice of the depth of the passive waveguide is not very sharp.

Another study has been done at the frequency used on Tore Supra (3.7 GHz) and we show on figs. 10 and 11 the influence of the short circuit position (l_{cc}) on the amplitude and on the phase of the electric field. This calculation has been performed assuming an array of 6 active waveguides alternating with 6 passive ones and for an electron density of 3.4×10^{11} cm^{-3}, an electron density gradient of $10^{12} cm^{-4}$ and a phase shift $2\varphi = 240°$. For the amplitude it can be observed that the optimum is obtained for a passive waveguide depth l_{cc} a little smaller than $\lambda/4$ which would be around 20 mm for this frequency (fig 10). This is due to the role of other waveguides which is not taken into account in (1) in evaluating the cross-coupling through the plasma. For the phase the optimum phase shift is 120° for l_{cc} = 16 mm. Far from this working point the phase shifts between consecutive waveguides show some variations which would lead to a degradation of the spectrum (fig 11).

3.4.Dependence of the results on the active waveguide phasing

Here the electron density is supposed to be twice the cutoff electron density and the electron density gradient is $7.3 \times 10^{11} cm^{-4}$. At the selected frequency of 5 GHz the coupling properties have been studied for the two geometric periodicities used before. Moreover, for the case Δ = 11.25 mm, two distinct passive waveguide depths were considered, l_{cc} = 12 and 16 mm. The phase shift variation between consecutive active waveguides, 2φ, was varied from 180 to 360 degrees. On fig. 12 the optimum value is obtained in the case Δ = 10 mm for 2φ = 240 degrees. For the other geometrical period, Δ = 11.25 mm, corresponding to a phase shift 2φ = 270 degrees, the reflection coefficient is lower than 1 % when the reflector waveguide depth is 16 mm. The maximum power directivity,

$\eta_p \approx 70$ %, is obtained when 2φ is between 240 and 270 degrees (fig. 13). The $N_{//}$ spectrum flexibility allowed by changing the driver phasing will be shown in section 3.7.

3.5.Dependence of the results on the septum thickness

3.5.1.Constant driver waveguide width

The septa which separate the reflector and driver waveguides will be subject to erosion from the plasma and therefore the launcher mouthpiece will need to be replaced from time to time. Increasing the thickness of these septa would then increase the lifetime of the antenna plasma facing component and also increase its thermal conductivity and robustness. The study of the influence of the septum thickness on the coupling and directivity properties of the antenna has been done for the case with a geometric periodicity $2\Delta = 22.5$ mm and a phase shift between the driver waveguides of 270 degrees. The width of the driver waveguides has been kept constant equal to 9.25 mm. When the passive waveguide width decreases the amplitude of the cross-coupling coefficient S_{12} decreases (fig. 14) leading therefore to a deterioration of the coupling properties up to a mean reflection coefficient of 9.5 % when the septum thickness is 5 mm (fig 15). For a septum width of 3 mm the reflection coefficient is smaller than 1%. The influence of this parameter on the antenna directivity is not significant (fig. 16).

3.5.2.Equal reflector and driver widths

Here the variation of the septum width is done at the expense of both the passive and the active waveguides. This is less advantageous than in the previous case because it will lead to an increase of the maximum electric field in the driver waveguides for a given incident power. As before, the amplitude of the cross-coupling coefficient S_{12} decreases when the waveguide width decreases (fig. 17). The coupling to the plasma shows a minimum when this width is around 8 mm (fig. 18). A slight increase of the launcher directivity is observed when the septum width increases (fig. 19).

3.6.Dependence of the results on the geometric periodicity of the array

The change of the geometric periodicity of the array will influence mainly the $N_{//peak}$ value. An increase of the period will lead to a decrease in the $N_{//}$ value of the main peak. For instance, changing the periodicity from 10 mm to 12 mm lowers the $N_{//peak}$ value from 2 to 1.7 for a phase shift between drivers (2φ) of 240 degrees. In the same time the amplitude of the cross-coupling coefficient through the plasma between neighbouring driver and reflector waveguides increases (fig. 20) leading to an increase of the electric field amplitude in the

passive waveguides, and therefore to an improvement of the coupling to the plasma (fig. 21). For the same reasons, the launcher directivity increases when Δ increases (fig. 22). In this study the septum thickness has been kept constant, therefore the variation of the periodicity means a change in the waveguide width.

3.7.The radiated $N_{//}$ power spectrum

On fig. 23 radiated $N_{//}$ spectra are shown for a case at twice the cutoff electron density, with an electron density gradient of $7.3 \times 10^{11} cm^{-4}$, a reflector waveguide depth of 16 mm and an array periodicity Δ = 11.25 mm. The phase between the driver waveguides (2φ) has been varied between 180° and 360°. It appears that the peaks corresponding to odd orders have disappeared for a large range of phasings due to the coherent amplitudes and phases in the active and passive waveguides. The launched spectra are therefore quite similar to those of present LH antennas.

When the phasing between neighbouring active waveguides, 2φ, is changed from 180 degrees to 360 degrees, the $N_{//}$ value of the main peak of the radiated spectrum is changing from 1.3 to 2.7.

3.8.Comparison of the total electric field in the reflector waveguide array and in a fully active waveguide antenna.

The use of active and passive waveguides leads to a decrease by a factor 2 of the available power transmission area. At first sight, this would mean that the radiated power for a given port area would be divided by 2. In fact, this is not quite correct as we shall see below. A computation of the maximum total electric field has been done for an active/passive waveguide array composed of 9 driver and 10 reflector waveguides, and compared with a 19-active-waveguide array. It can be observed that for the selected electron density (twice the cutoff density) and electron density gradient (7.3×10^{11} cm^{-4}), the total electric field is lower with the active/passive waveguide array because of a better coupling.

Thus, if the limiting factor for power transmission is the maximum tolerable electric field in the waveguides, then the amount of power which can be delivered by a reflector waveguide array can be more than half the power delivered by a fully active waveguide array. Using the average value of the total electric field in the waveguides ones finds that the amount of power which could be delivered to the plasma would be around 60 to 75 % of the power capability of a fully active waveguide antenna (fig. 24). On the other hand, if the power handling limitations of LH launchers are due to the electric fields at the plasma edge and therefore to the coupled power density per unit area of the launcher mouthpiece, then reflector waveguide arrays may even have a better power handling capability.

4.CONCLUSION

The concept of a "reflector waveguide array" is proposed for the plasma facing component of an advanced LH launcher. It falls into the general category of reflector antennas and it has been shown in our studies that the power spectrum radiated by such a structure can have a power directivity and a coupling efficiency similar to present-day LHCD antennas.

Moreover, it has been shown that the coupling properties of such an antenna are optimized at low edge density where the thermal load is lower. It has also been shown that the choice of the optimum depth for the passive waveguides ($\approx \lambda/4$) is not very sharp and that the phase shift between the active driver waveguides can be changed giving the required power spectrum flexibility with good coupling properties. The thickness of the septa which separate the driver and reflector waveguides can be increased to better withstand the plasma erosion without a large degradation of the coupling properties and of the radiated $N_{//}$ spectrum.

The reflector waveguide array can be fed in several ways, e.g. by hyperguides and/or mode converters. It is indeed ideally suited for being used in conjunction with poloidally oversized waveguides. By allowing a large reduction of the total number of waveguides without decreasing the mechanical strength of the structure, such a combination yields a simplified and more robust LH launcher which can be easily water cooled through pipes situated in the thick walls behind the passive reflector waveguides. If necessary, multijunctions can be used to further reduce the reflection coefficient and therefore make an optimum use of components such as hyperguides and mode converters which need to be properly matched.

Because it is a very dense structure, the reflector waveguide array offers a very good neutron shielding through the occupied port. Nevertheless, the total amount of power which can be delivered to the plasma should reach 60-75 % of the one delivered by a fully active - but neutron transparent - waveguide launcher occupying the same port area. This ratio can perhaps be even higher if the limitation comes from the coupled power density at the plasma edge.

Reflector waveguide arrays can therefore be quite advantageous for applying LH waves in the next step reactor-grade tokamaks.

ACKNOWLEDGEMENTS

We acknowledge fruitful discussions within the European Coordinating Committee for Lower Hybrid Waves (CCLH) regarding the integration of this concept in an ITER launcher.

REFERENCES.

[1] NET Predesign report by NET Team. Fusion Engineering and Design, vol. **21** (1993) 298.

[2] M. Pain, *et al.*, "The Hyperguide : a new concept of Lower Hybrid Launcher", Report JET-P (92) 94, JET Joint Undertaking, Abingdon (U.K.), November 1992.

[3] Y. Ikeda, *et al.*, "The Upgrade of the 2 GHz LHCD system on the JT-60U", Proceedings of the 17th Symposium on Fusion Technology, Rome (Italy), 14-18th september 1992.

[4] Ph. Bibet, T.K. Nguyen, "Experimental and theoretical results concerning the development of the main RF components for next Tore Supra LHCD antennae", Proceedings of the 18th Symposium on Fusion Technology, Karlsruhe (Germany), 22-26th August 1994.

[5] M.I. Petelin, E.V. Suvorov, Pisma v. Zhtf (letters to journal of Technical physics), vol. **15** (1989) 23.

[6] J.P. Crenn, Ph. Bibet, "Quasi-optical grill using difraction gratings for Lower Hybrid waves systems", Report EUR-CEA-FC-1508, Centre d'Etudes de Cadarache, France (1994).

[7] Ph. Bibet, X. Litaudon, D. Moreau, "Principle of a 'retro-reflecting' or 'backfire' LH antenna", IAEA Technical Committee Meeting on RF launchers for Plasma Heating and Current Drive, Naka (Japan), 10-12th November 1993.

[8] D. Moreau, T.K. NGuyen, "Couplage de l'onde lente au voisinage de la fréquence hybride basse dans les grands tokamaks", Report EUR-CEA-FC-1246, Centre d'Etudes Nucléaires de Grenoble, France (1984).

[9] X. Litaudon, D. Moreau, Nuclear Fusion **30** (1990) 471.

[10] X. Litaudon, *et al.*, Nuclear Fusion **32** (1992) 1883.

FIGURE CAPTIONS

figure 1 : sketch of a reflector waveguide array.

figure 2 : cross-coupling coefficient S_{12} vs electron density.

figure 3 : mean reflection coefficient R vs electron density.

figure 4 : power directivity, η_p, and $N_{//}$-weighted directivity for $N_{//peak} = 2$, η_{cd}, vs electron density.

figure 5 : cross-coupling coefficient S_{12} vs electron density gradient.

figure 6 : mean reflection coefficient R vs electron density gradient.

figure 7 : power directivity, η_p, and $N_{//}$-weighted directivity for $N_{//peak} = 2$, η_{cd}, vs electron density gradient.

figure 8 : mean reflection coefficient R vs passive waveguide depth, l_{cc}.

figure 9 : power directivity, η_p, and $N_{//}$-weighted directivity for $N_{//peak} = 2$, η_{cd}, vs passive waveguide depth, l_{cc}.

figure 10 : amplitude of the electric field of the fundamental mode vs passive waveguide depth and the number of the waveguide.

figure 11 : phase of the electric field of the main mode vs the passive waveguide depth and the number of the waveguide.

figure 12 : mean reflection coefficient R vs phase shift between active waveguides, 2φ.

figure 13 : power directivity, η_p, vs phase shift between active waveguides, 2φ.

figure 14 : cross-coupling coefficient S_{12} vs septum width. The active waveguide width is kept constant equal to 9.25 mm.

figure 15 : mean reflection coefficient R vs septum width.

figure 16 : power directivity, η_p, and $N_{//}$-weighted directivity for $N_{//peak} = 2$, η_{cd}, vs septum width.

figure 17 : cross-coupling coefficient S_{12} vs waveguide width, b. The driver waveguide width is supposed equal to the reflector waveguide width.

figure 18 : mean reflection coefficient R vs waveguide width.

figure 19 : power directivity, η_p, and $N_{//}$-weighted directivity for $N_{//peak} = 2$, η_{cd}, vs waveguide width.

figure 20 : cross-coupling coefficient S_{12} vs geometric periodicity. The septum thickness is kept constant equal to 2 mm.

figure 21 : mean reflection coefficient R vs geometric periodicity.

figure 22 : power directivity, η_p, vs geometric periodicity.

figure 23 : Radiated $N_{//}$ power spectra for various phase shifts between the driver waveguides.

figure 24 : Ratio of the total electric field at the interface plasma/antenna of a reflector array composed of 9 active waveguides and 10 passive ones, to the same electric field for a 19-active-waveguide coupler.

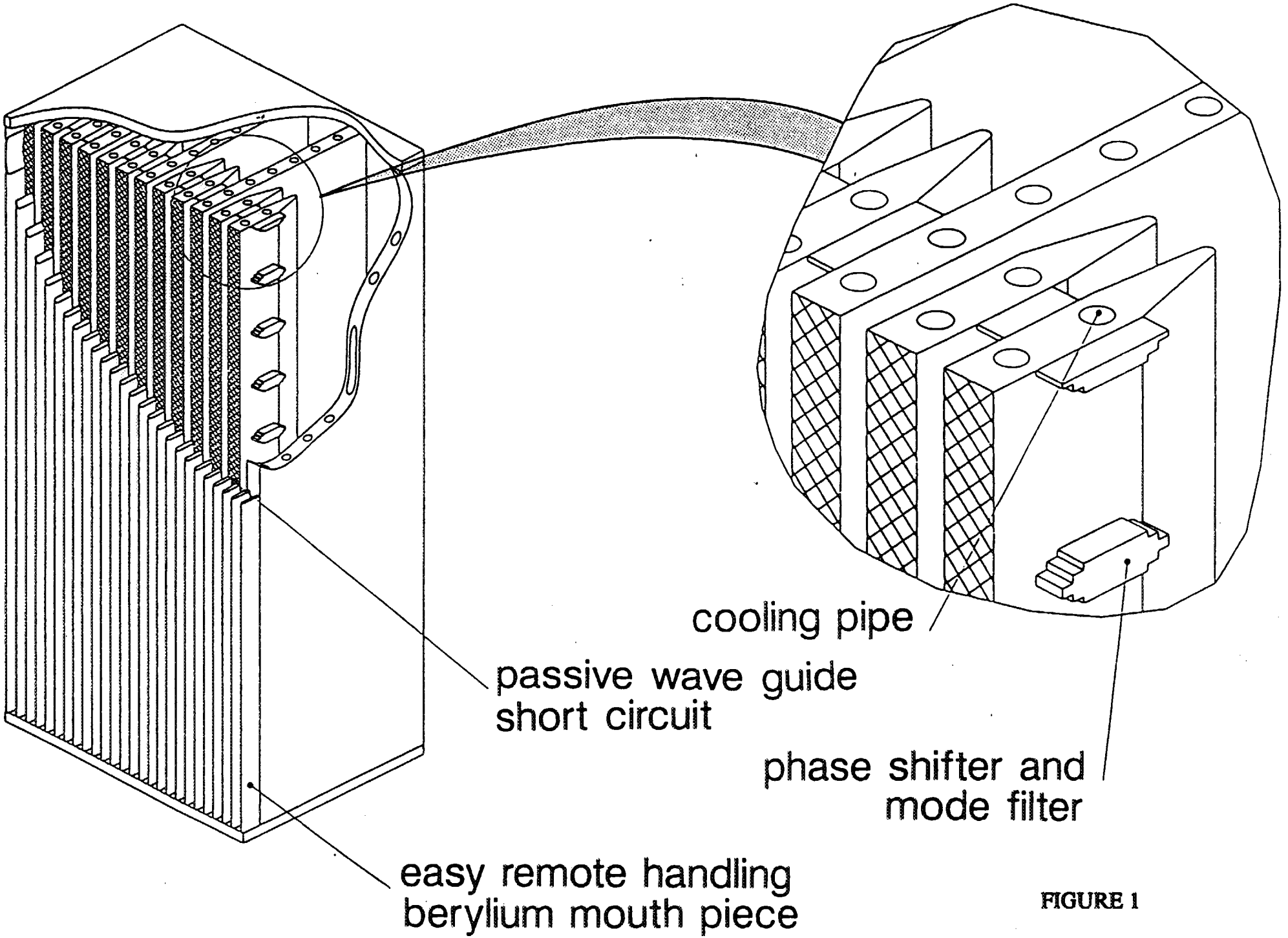
cooling pipe
passive wave guide
short circuit
phase shifter and
mode filter
easy remote handling
berylium mouth piece

FIGURE 1

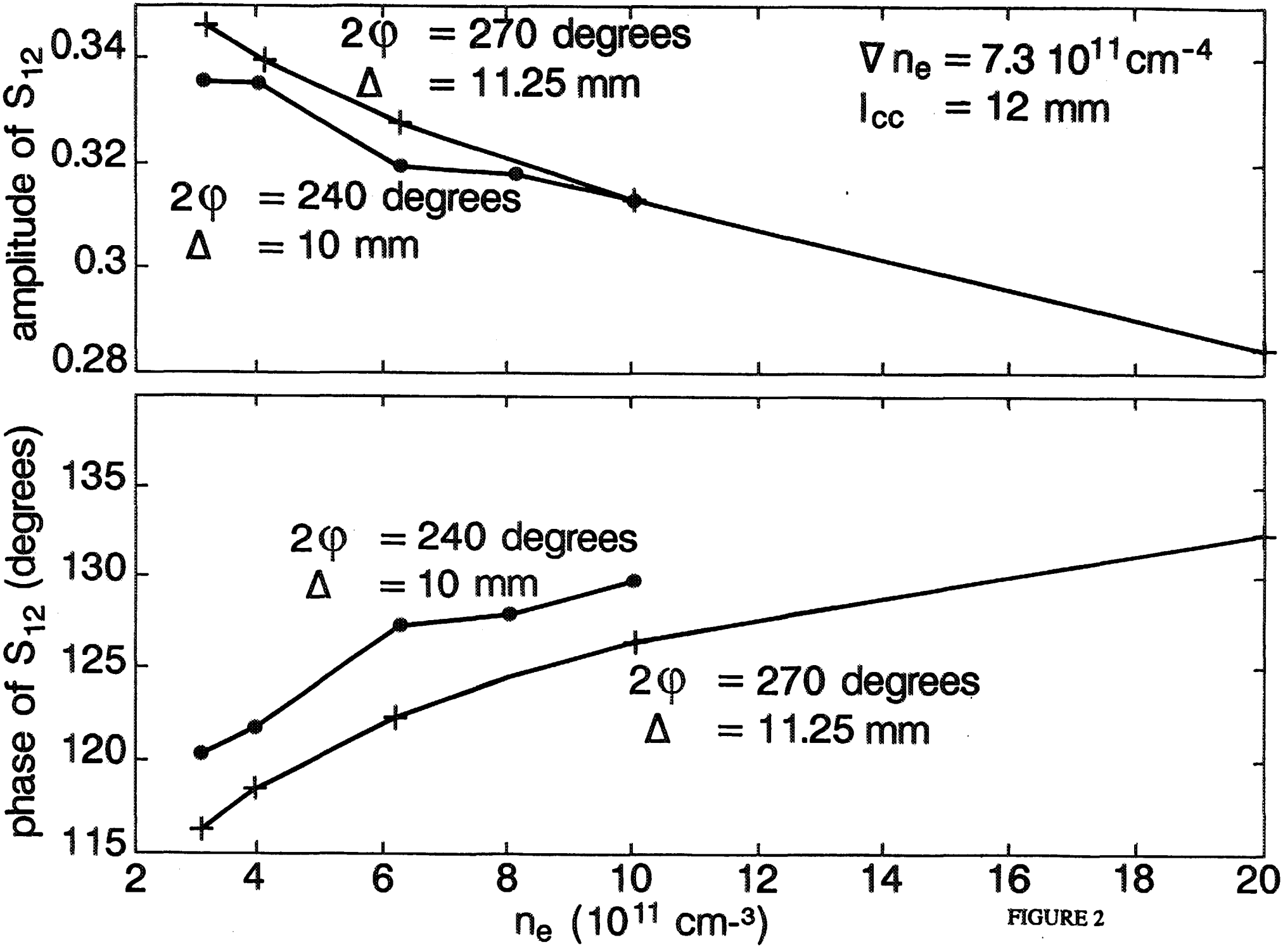
amplitude of S_{12}
0.34
0.32
0.3
0.28
2φ = 270 degrees
Δ = 11.25 mm
$\nabla n_e = 7.3\ 10^{11} cm^{-4}$
l_{cc} = 12 mm
2φ = 240 degrees
Δ = 10 mm
phase of S_{12} (degrees)
135
130
125
120
115
2φ = 240 degrees
Δ = 10 mm
2φ = 270 degrees
Δ = 11.25 mm
2
4
6
8
10
12
14
16
18
20
n_e (10^{11} cm^{-3})

FIGURE 2

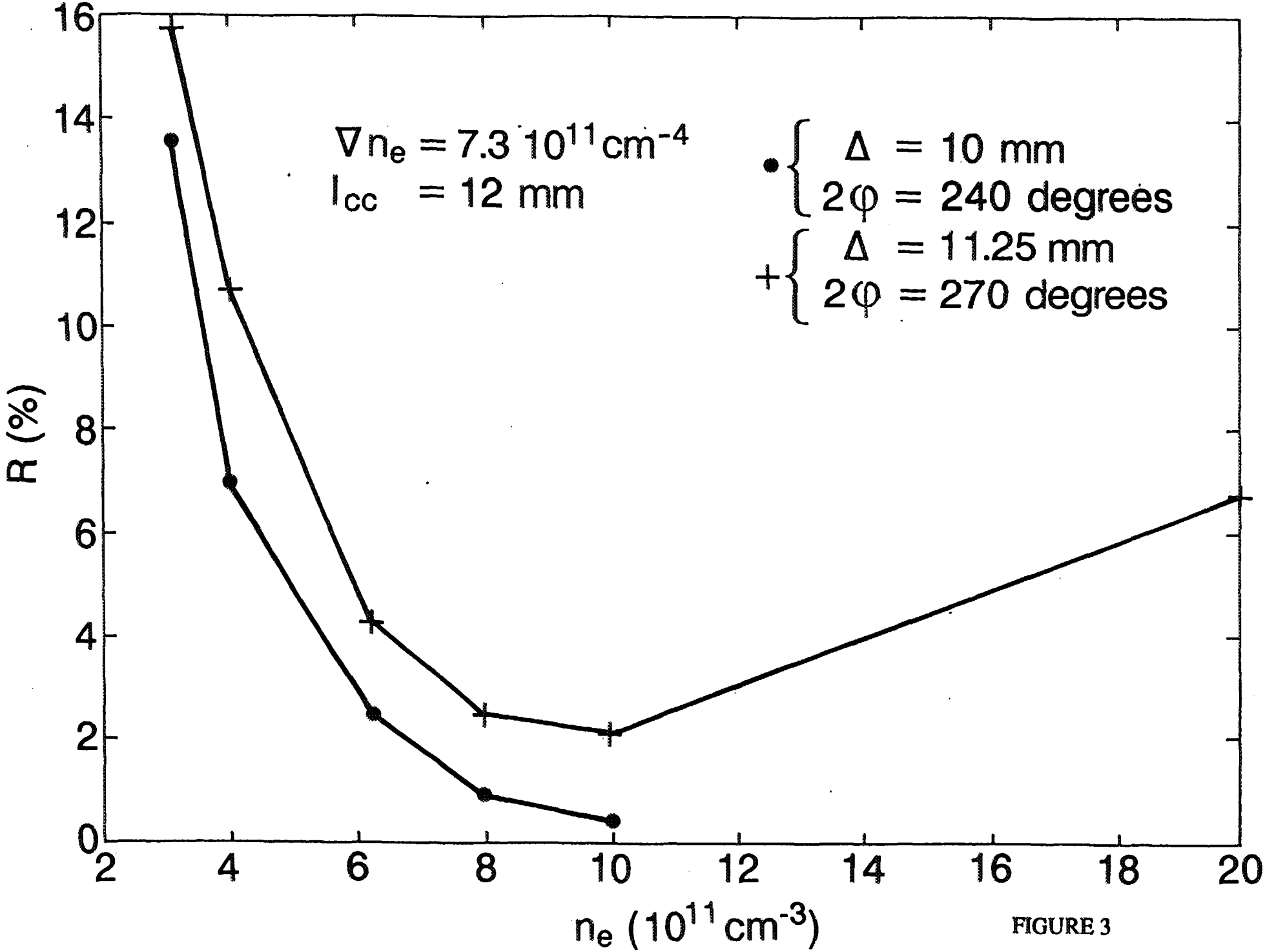
$\nabla n_e = 7.3\ 10^{11} cm^{-4}$
$l_{cc} = 12$ mm
$\Delta = 10$ mm
$2\varphi = 240$ degrees
$\Delta = 11.25$ mm
$2\varphi = 270$ degrees
R (%)
$n_e\ (10^{11} cm^{-3})$
0
2
4
6
8
10
12
14
16
18
20

FIGURE 3

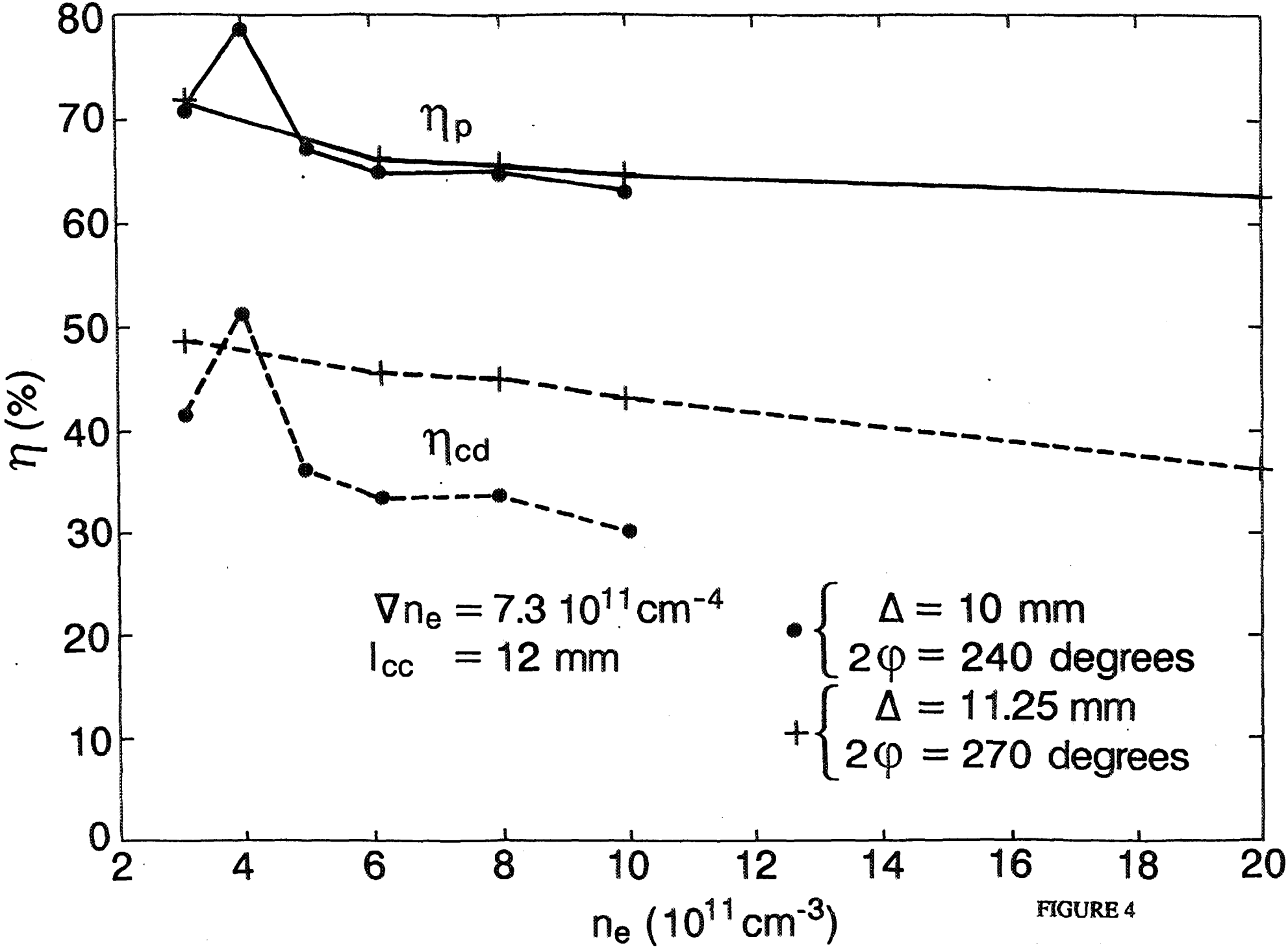
80
70
60
50
40
30
20
10
0
η (%)
η_p
η_{cd}
$\nabla n_e = 7.3\ 10^{11} cm^{-4}$
$l_{cc} = 12$ mm
• { Δ = 10 mm, 2φ = 240 degrees
+ { Δ = 11.25 mm, 2φ = 270 degrees
2
4
6
8
10
12
14
16
18
20
n_e ($10^{11} cm^{-3}$)

FIGURE 4

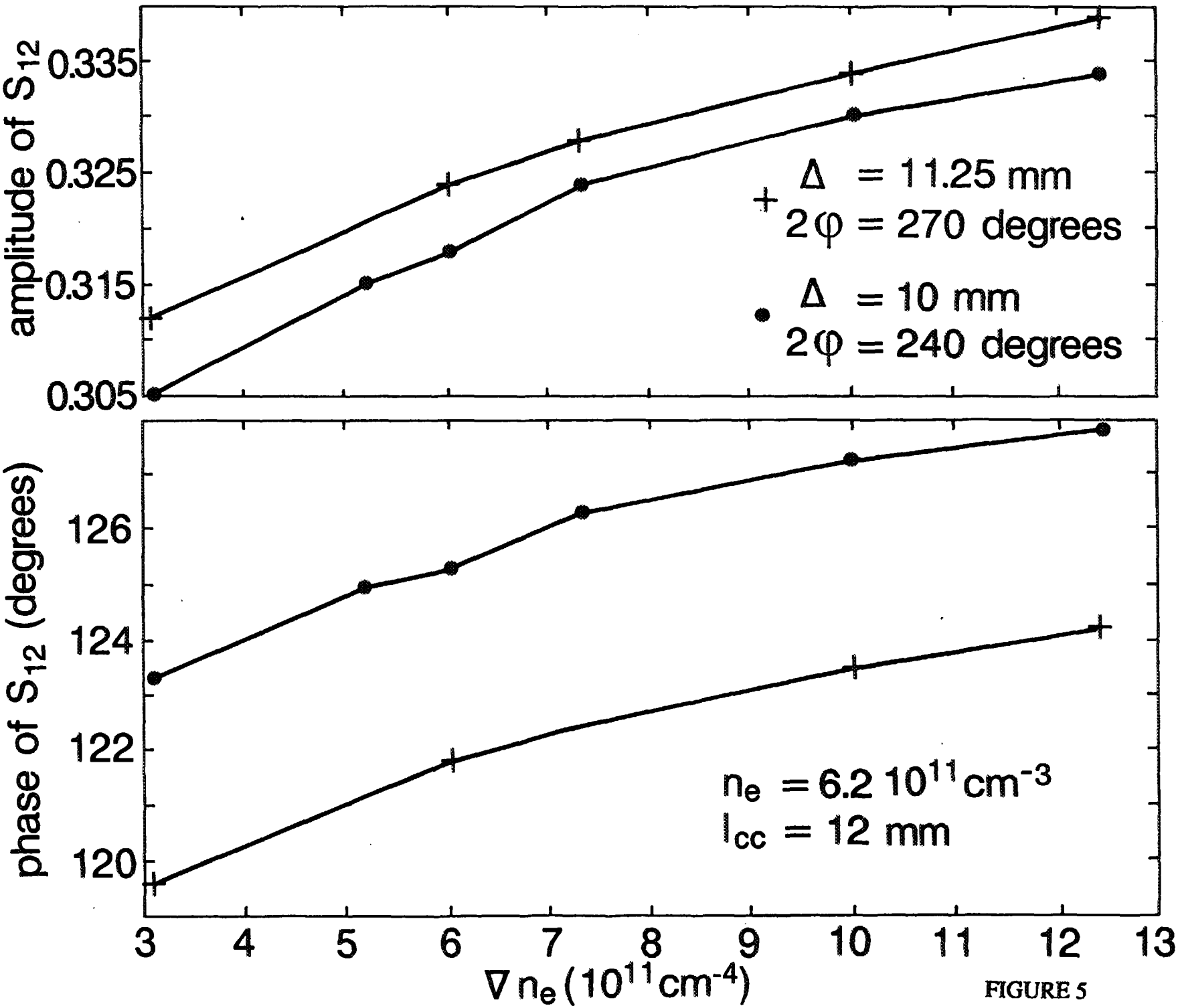
amplitude of S_{12}
0.335
0.325
0.315
0.305
Δ = 11.25 mm
2φ = 270 degrees
Δ = 10 mm
2φ = 240 degrees
phase of S_{12} (degrees)
126
124
122
120
$n_e = 6.2\ 10^{11} cm^{-3}$
l_{cc} = 12 mm
3
4
5
6
7
8
9
10
11
12
13
$\nabla n_e (10^{11} cm^{-4})$

FIGURE 5

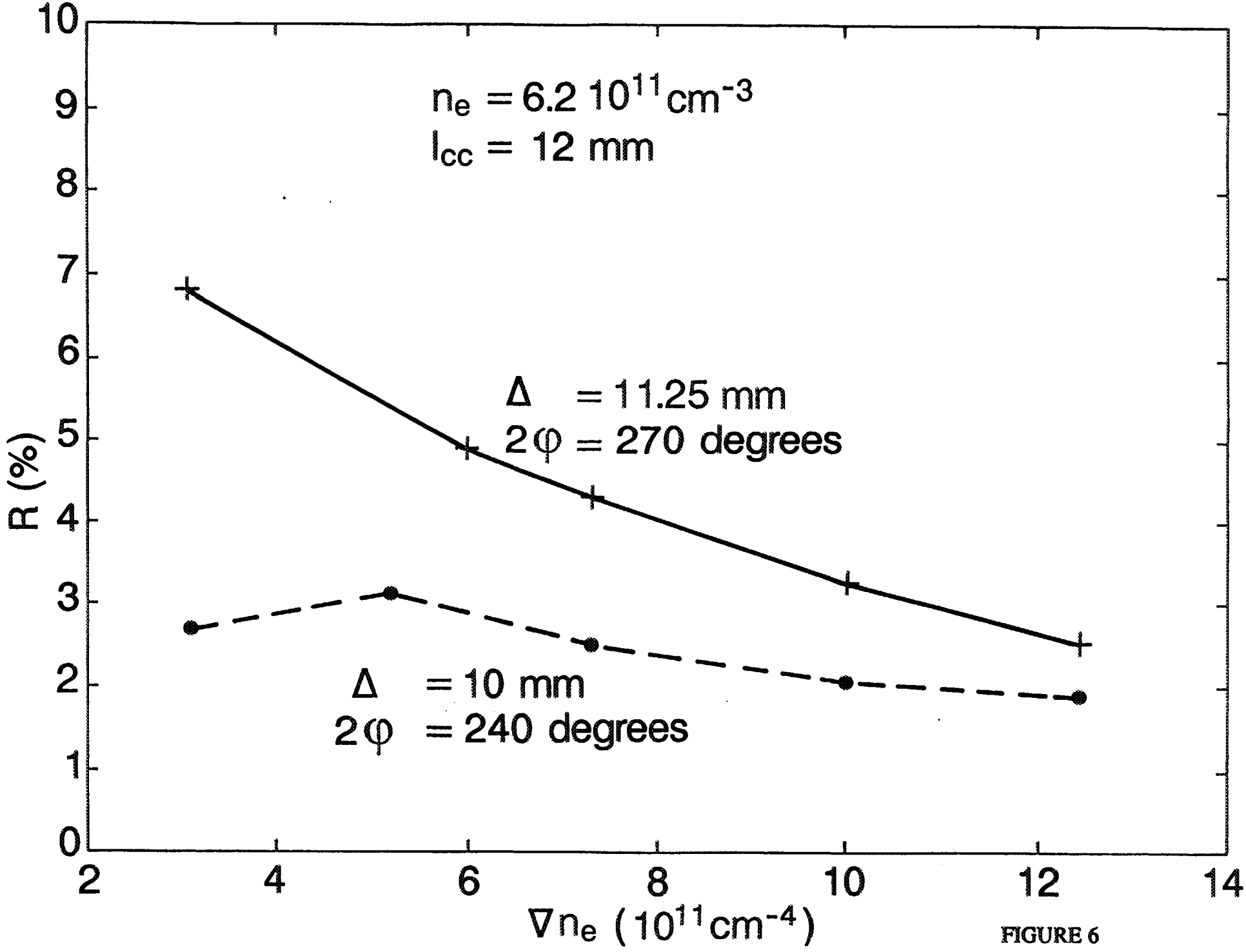
$n_e = 6.2\ 10^{11} cm^{-3}$
$l_{cc} = 12$ mm
$\Delta = 11.25$ mm
$2\varphi = 270$ degrees
$\Delta = 10$ mm
$2\varphi = 240$ degrees
R (%)
$\nabla n_e\ (10^{11} cm^{-4})$
0
1
2
3
4
5
6
7
8
9
10
2
4
6
8
10
12
14

FIGURE 6

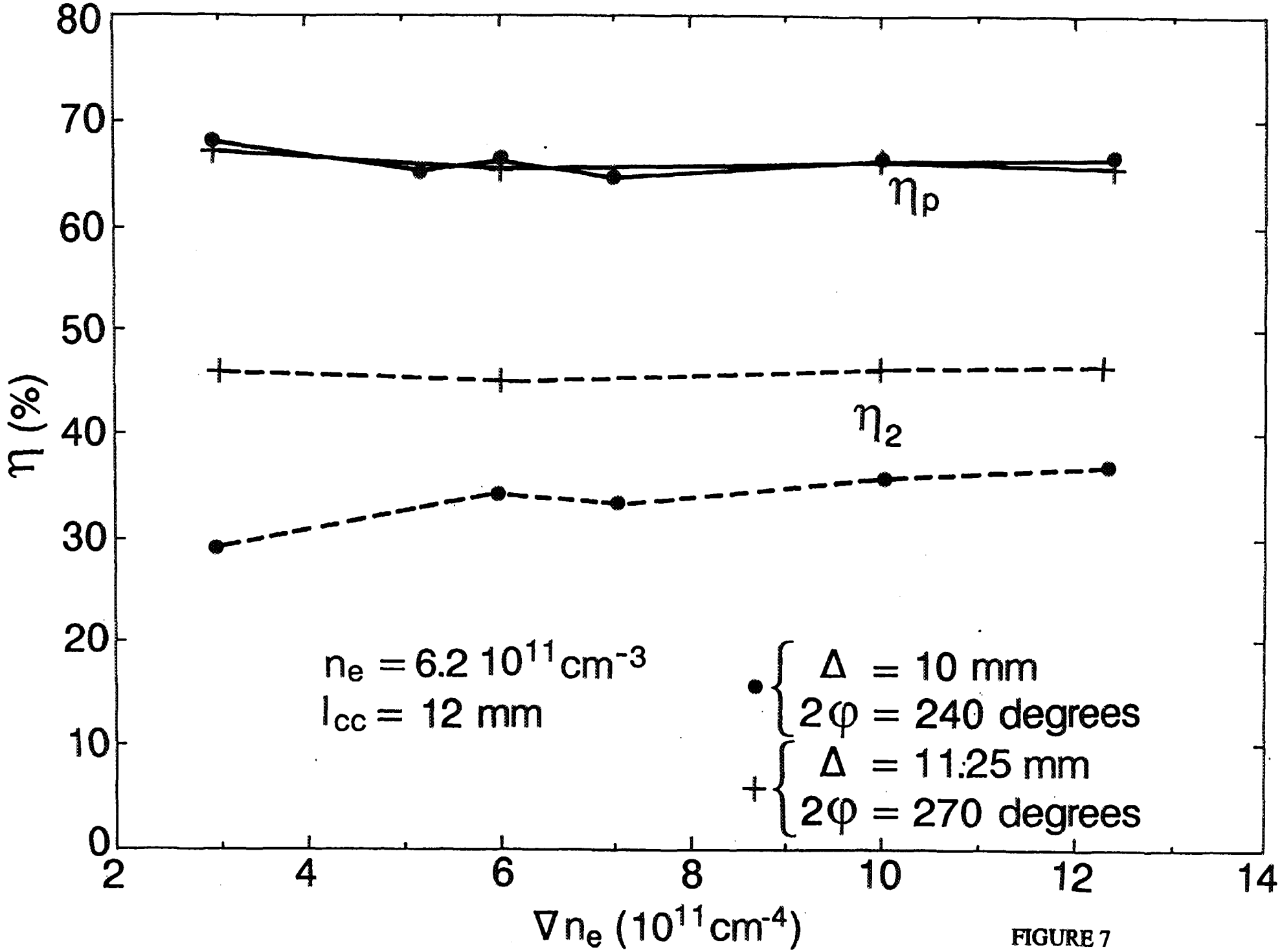
80
70
60
50
40
30
20
10
0
η (%)
2
4
6
8
10
12
14
∇ne (10^11 cm^-4)
ηp
η2
ne = 6.2 10^11 cm^-3
lcc = 12 mm
Δ = 10 mm
2φ = 240 degrees
Δ = 11.25 mm
2φ = 270 degrees

FIGURE 7

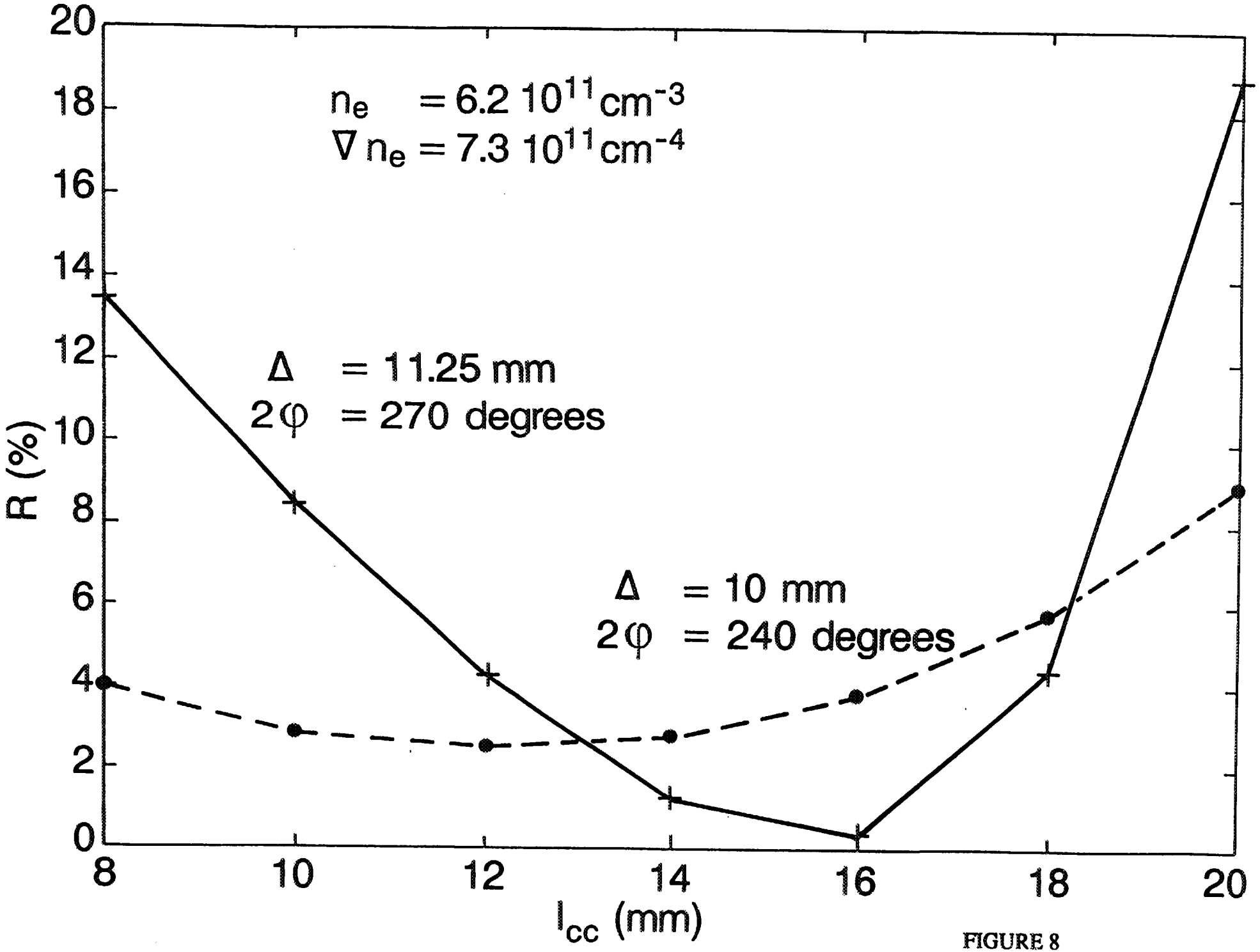
$n_e = 6.2\ 10^{11} cm^{-3}$
$\nabla n_e = 7.3\ 10^{11} cm^{-4}$
$\Delta = 11.25$ mm
$2\varphi = 270$ degrees
$\Delta = 10$ mm
$2\varphi = 240$ degrees
R (%)
l_{cc} (mm)
0
2
4
6
8
10
12
14
16
18
20
8
10
12
14
16
18
20

FIGURE 8

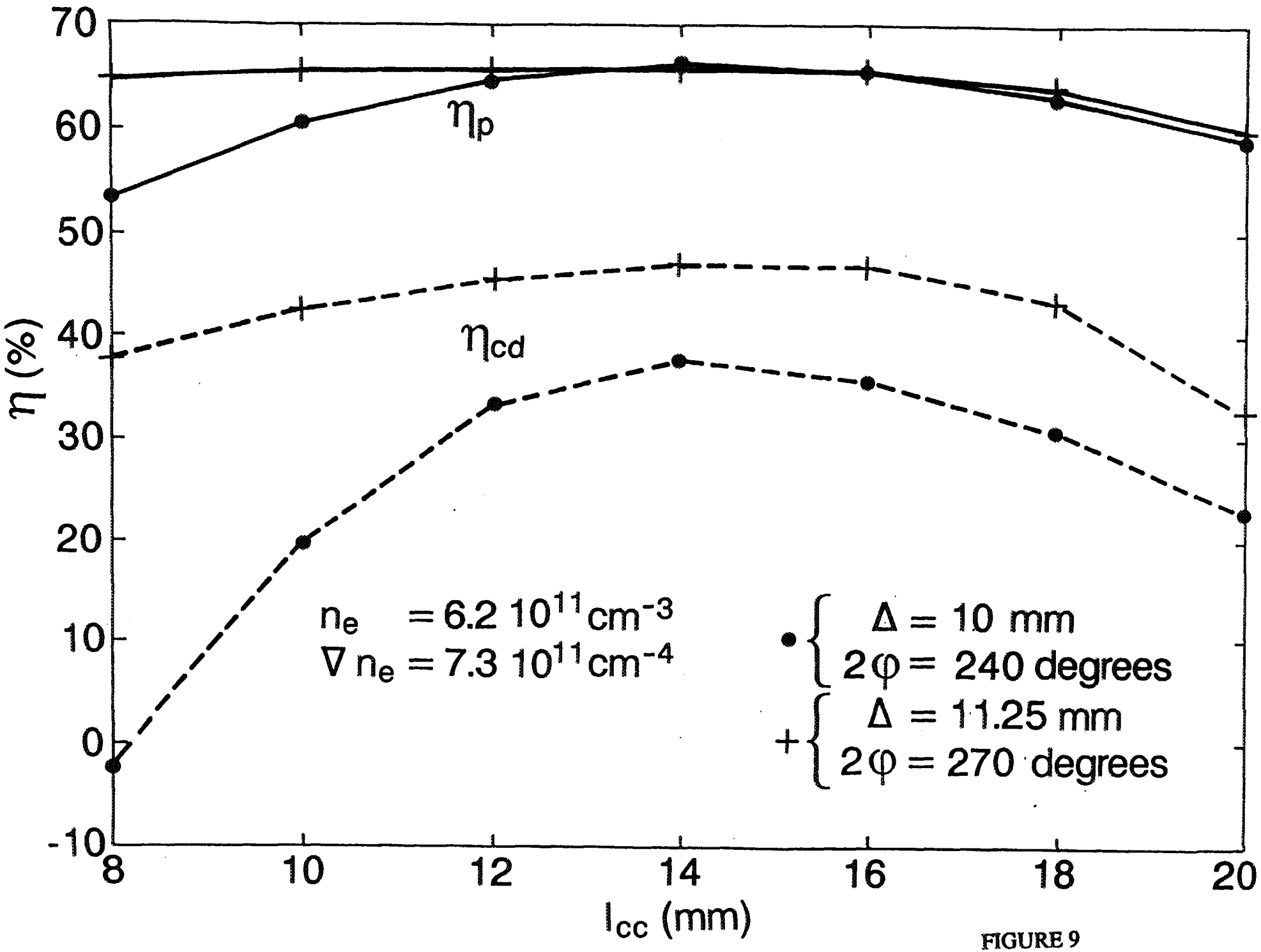
70
60
50
40
30
20
10
0
-10
8
10
12
14
16
18
20
η (%)
l_{cc} (mm)
η_p
η_{cd}
$n_e = 6.2\ 10^{11} cm^{-3}$
$\nabla n_e = 7.3\ 10^{11} cm^{-4}$
• Δ = 10 mm
2φ = 240 degrees
+ Δ = 11.25 mm
2φ = 270 degrees

FIGURE 9

FIGURE 10

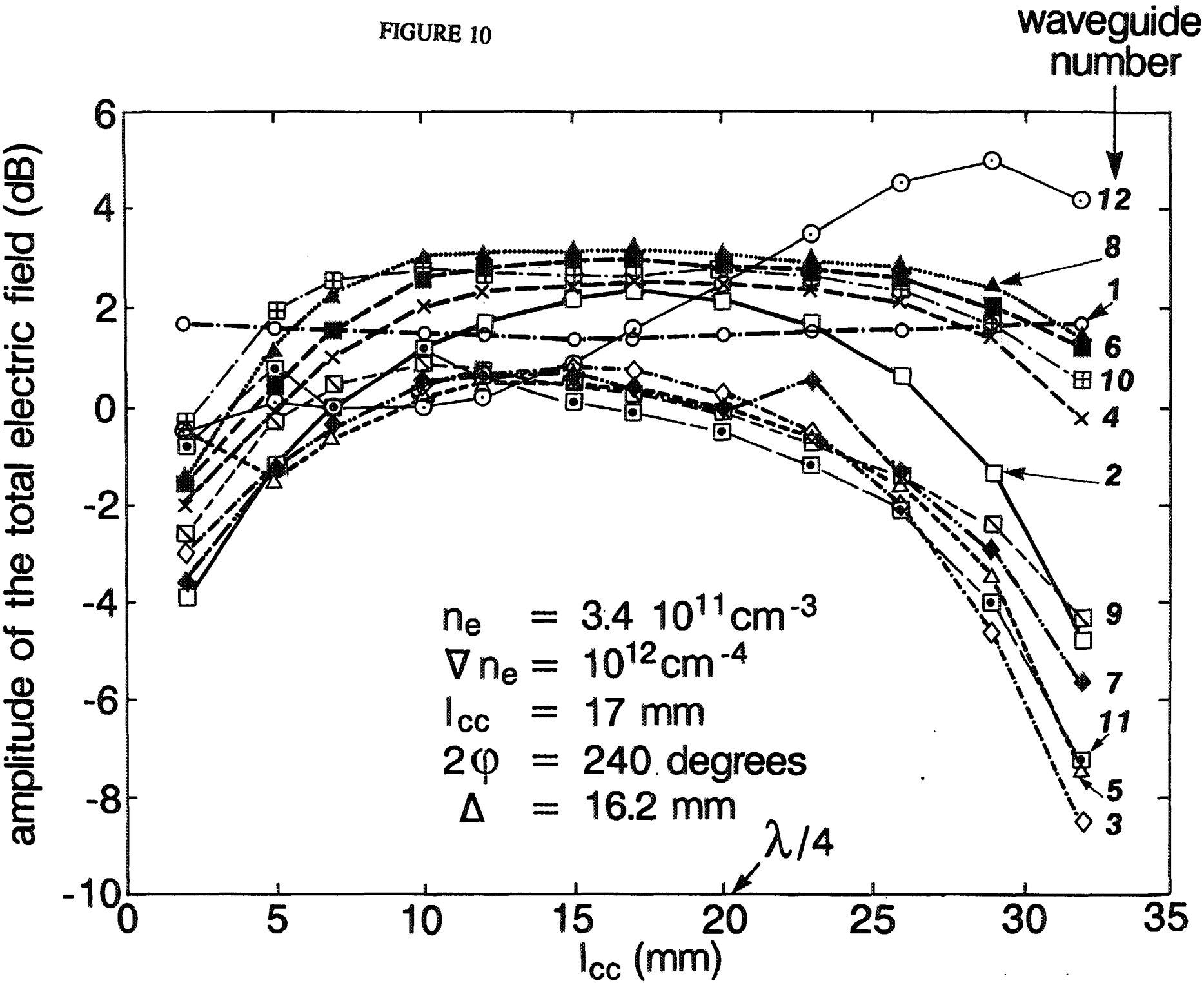
waveguide number
amplitude of the total electric field (dB)
6
4
2
0
-2
-4
-6
-8
-10
0
5
10
15
20
25
30
35
l_{cc} (mm)
12
8
1
6
10
4
2
9
7
11
5
3
n_e = 3.4 10^{11}cm^{-3}
∇n_e = 10^{12}cm^{-4}
l_{cc} = 17 mm
2φ = 240 degrees
Δ = 16.2 mm
λ/4

FIGURE 11

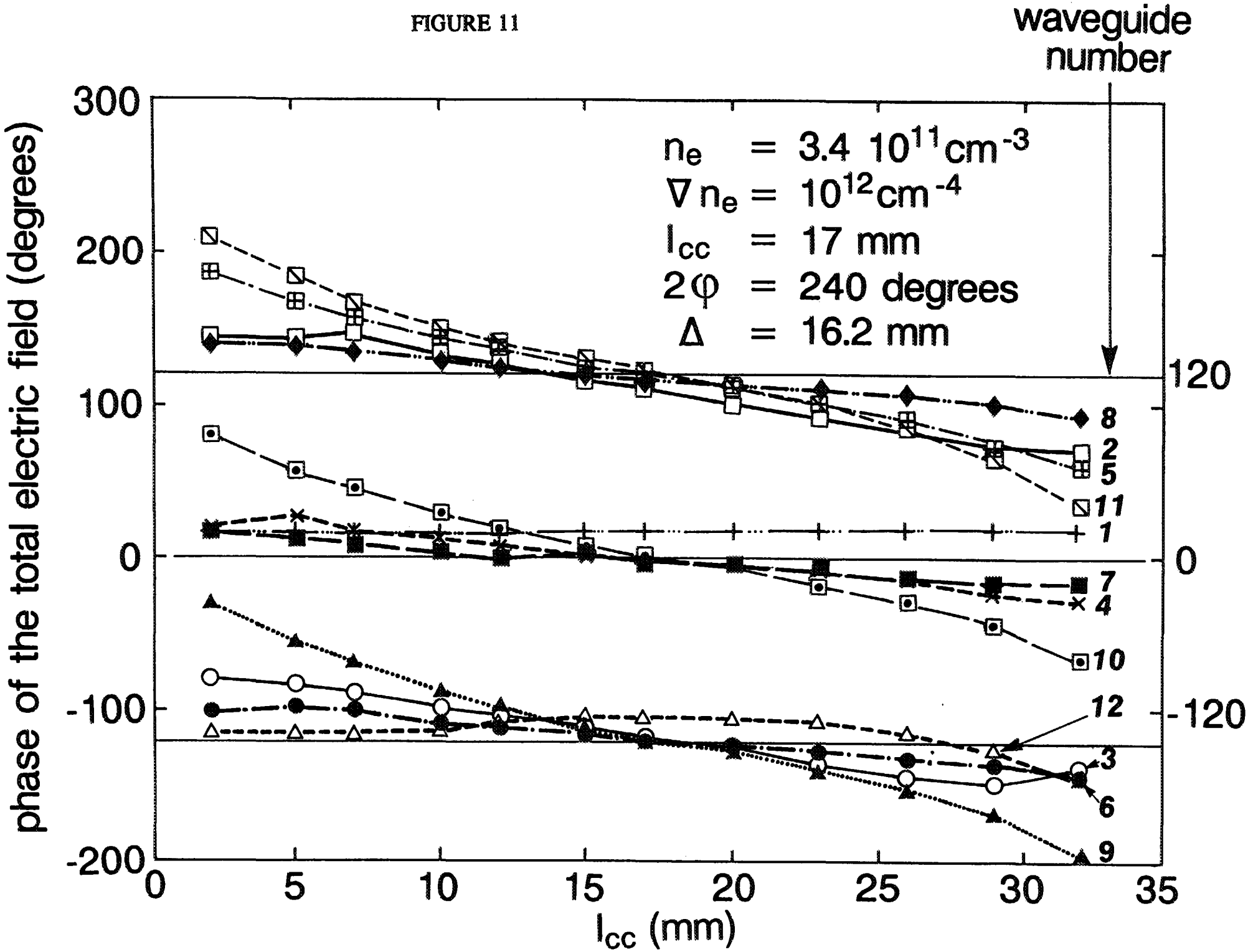
waveguide number
$n_e = 3.4\ 10^{11} cm^{-3}$
$\nabla n_e = 10^{12} cm^{-4}$
$l_{cc} = 17$ mm
$2\varphi = 240$ degrees
$\Delta = 16.2$ mm
phase of the total electric field (degrees)
l_{cc} (mm)
300
200
100
0
-100
-200
0
5
10
15
20
25
30
35
120
0
-120
8
2
5
11
1
7
4
10
12
3
6
9

FIGURE 12

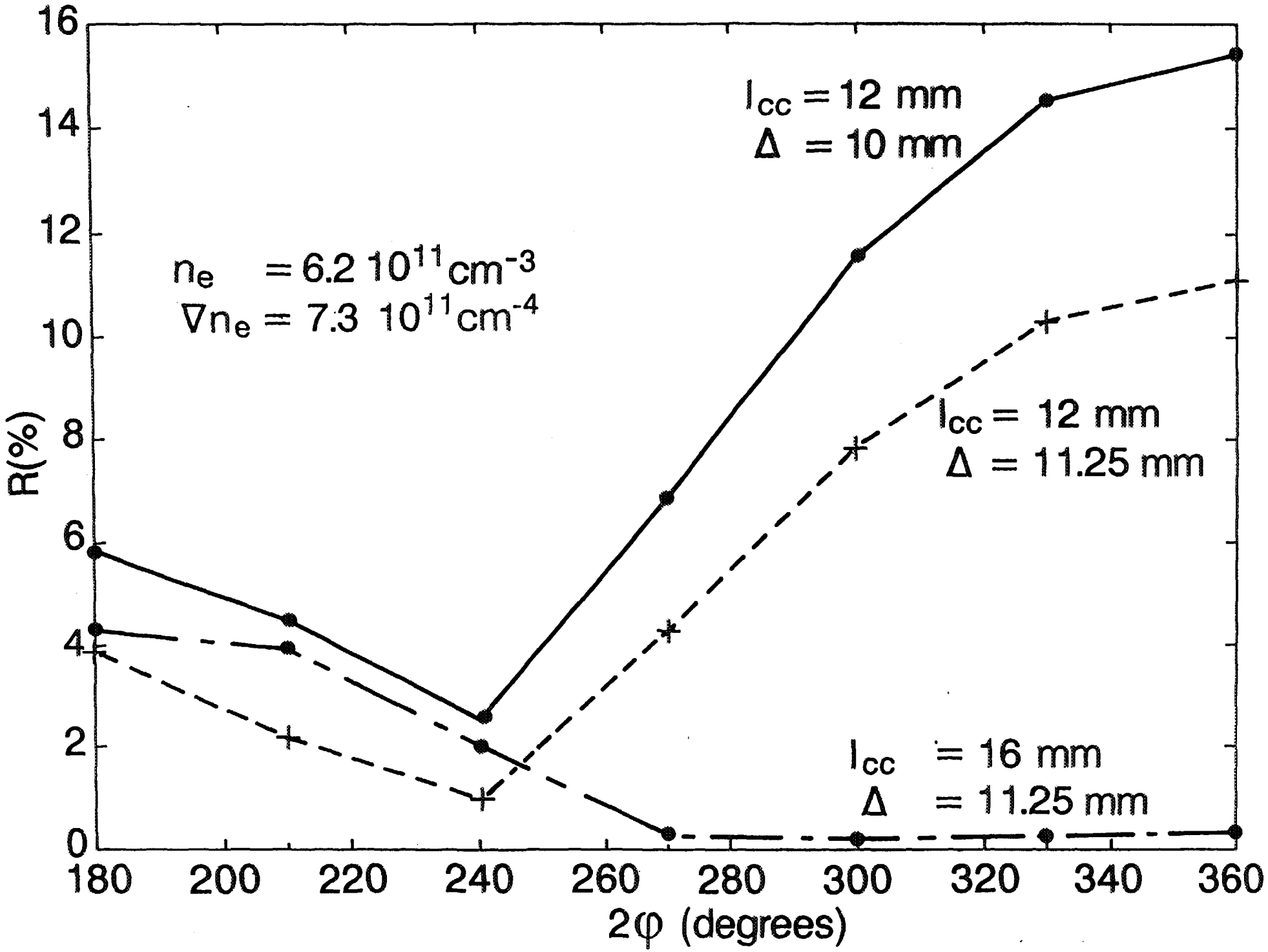
16
14
12
10
8
6
4
2
0
R(%)
180
200
220
240
260
280
300
320
340
360
2φ (degrees)
l_{cc} = 12 mm
Δ = 10 mm
n_e = 6.2 10^{11}cm^{-3}
∇n_e = 7.3 10^{11}cm^{-4}
l_{cc} = 12 mm
Δ = 11.25 mm
l_{cc} = 16 mm
Δ = 11.25 mm

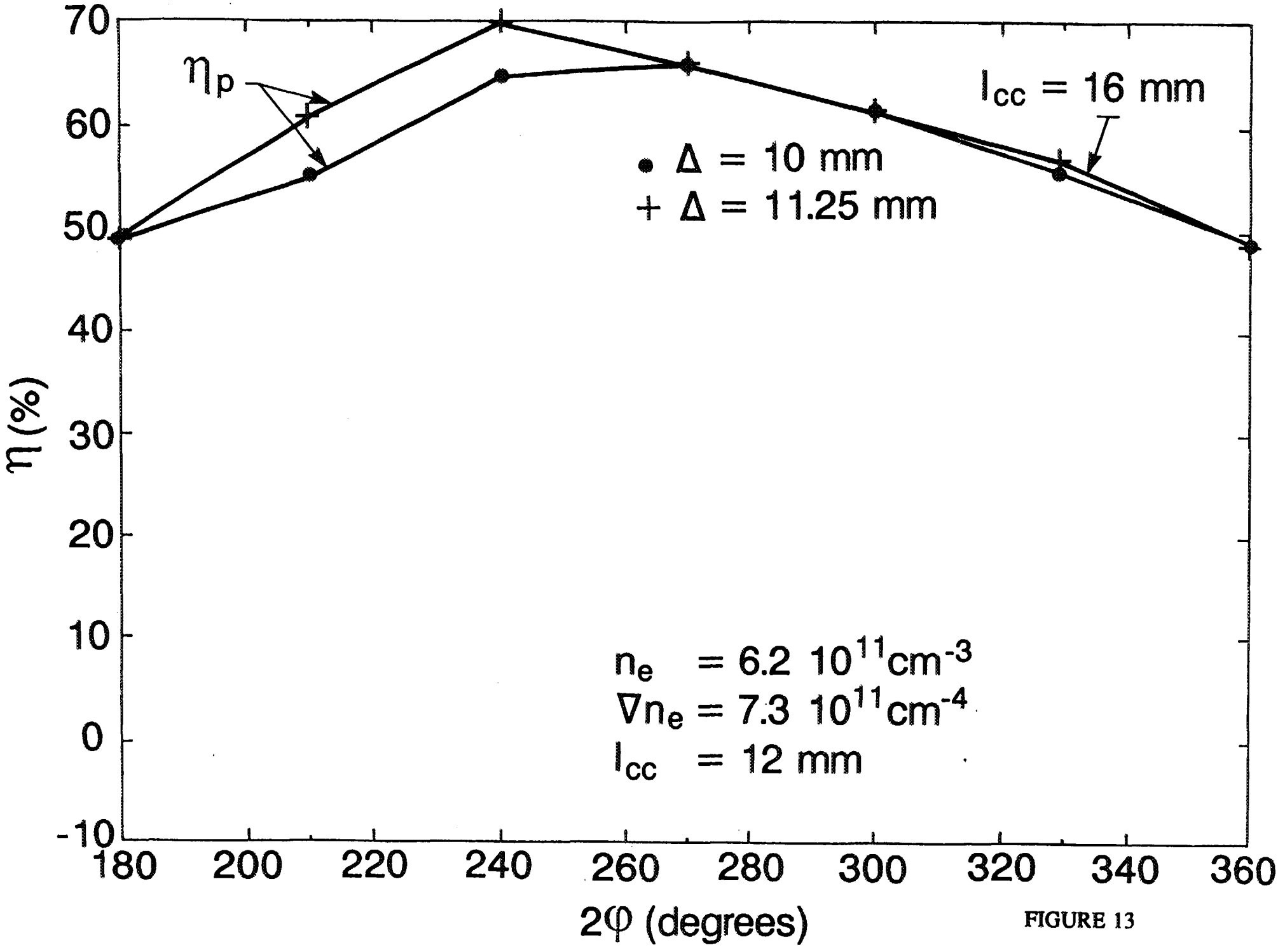
70
60
50
40
30
20
10
0
-10
180
200
220
240
260
280
300
320
340
360
η (%)
2φ (degrees)
ηp
Icc = 16 mm
• Δ = 10 mm
+ Δ = 11.25 mm
ne = 6.2 10^11 cm^-3
∇ne = 7.3 10^11 cm^-4
Icc = 12 mm

FIGURE 13

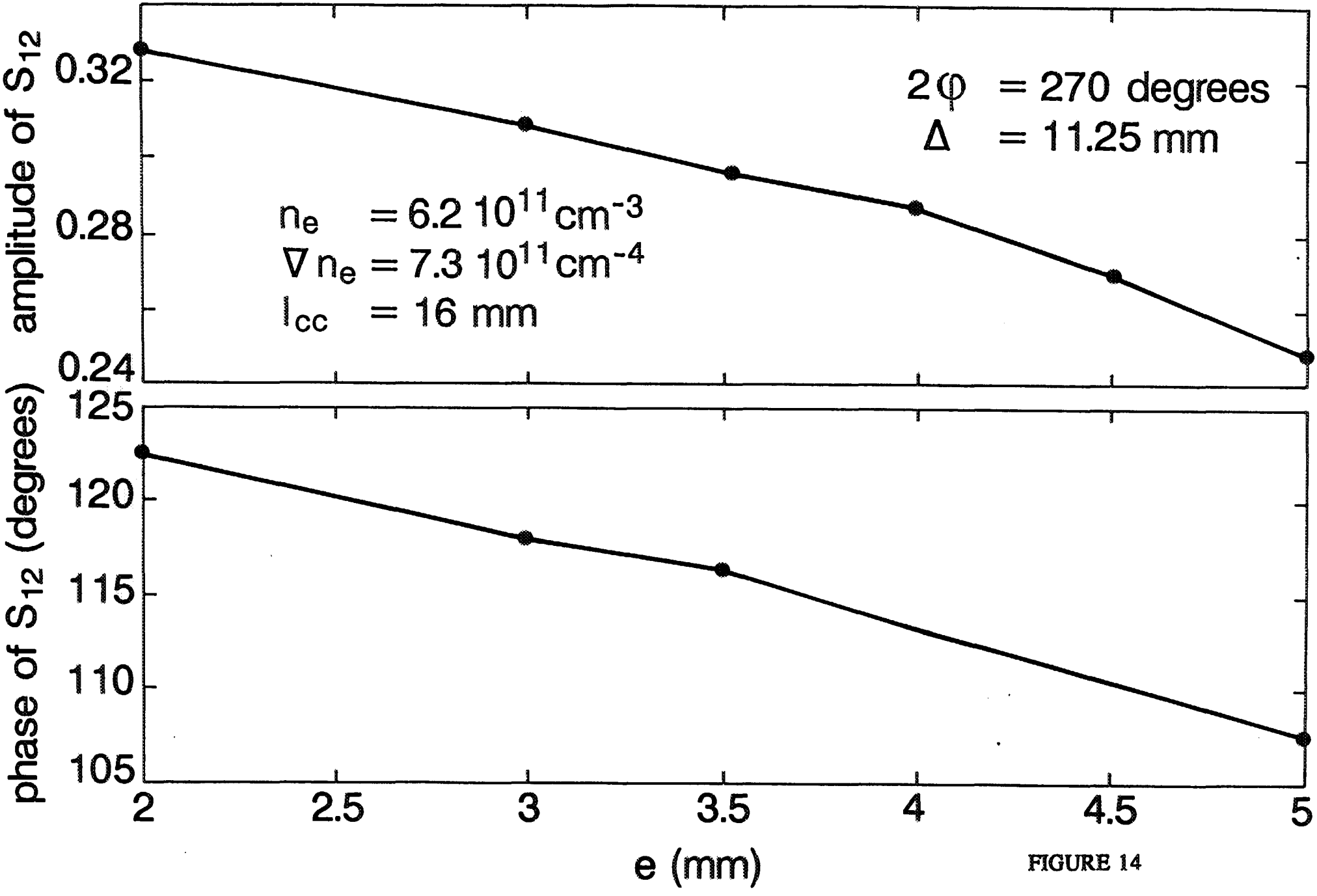
amplitude of S_{12}
0.32
0.28
0.24
2φ = 270 degrees
Δ = 11.25 mm
n_e = 6.2 10^{11} cm^{-3}
∇n_e = 7.3 10^{11} cm^{-4}
l_{cc} = 16 mm
phase of S_{12} (degrees)
125
120
115
110
105
2
2.5
3
3.5
4
4.5
5
e (mm)

FIGURE 14

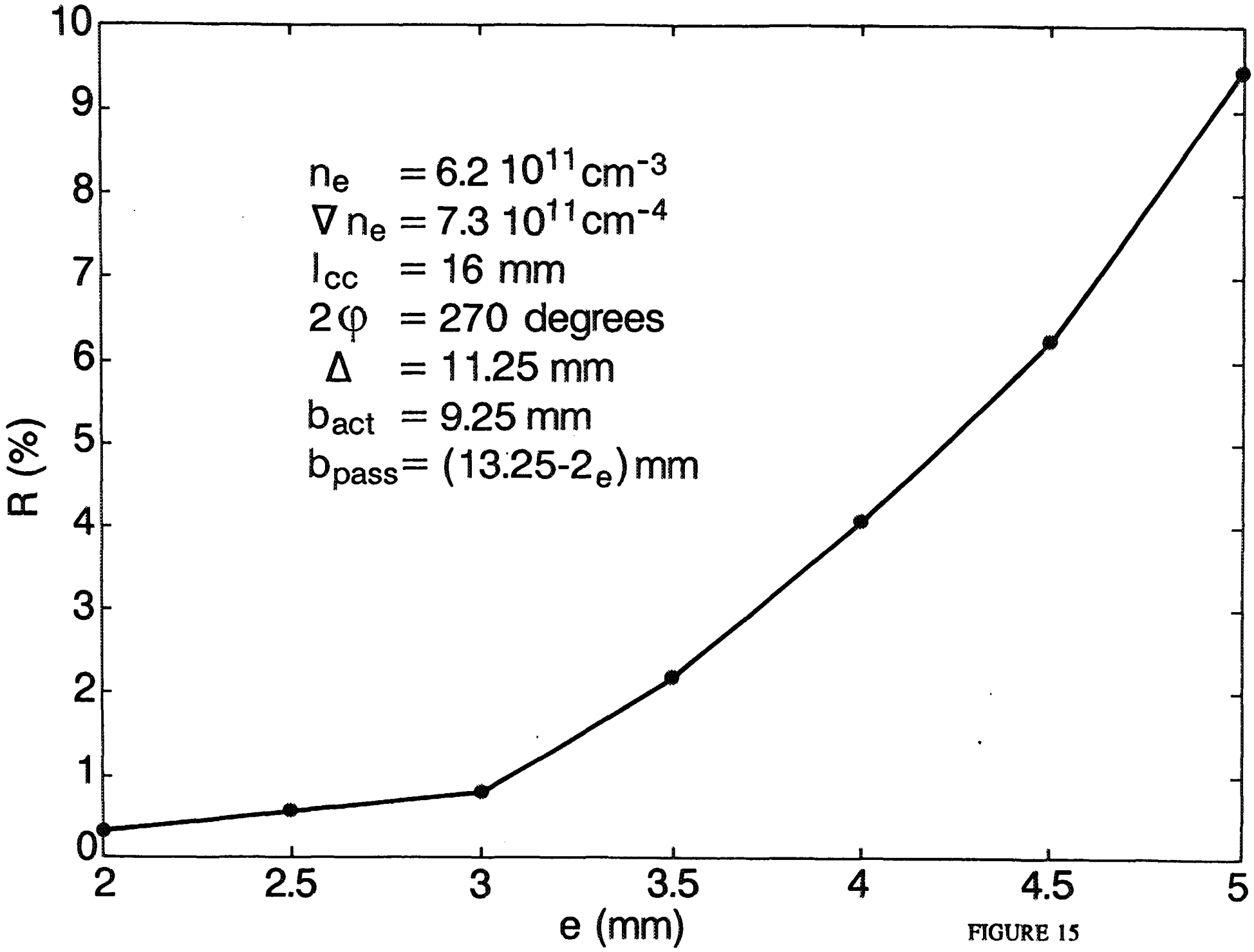
$n_e = 6.2\ 10^{11} cm^{-3}$
$\nabla n_e = 7.3\ 10^{11} cm^{-4}$
$l_{cc} = 16$ mm
$2\varphi = 270$ degrees
$\Delta = 11.25$ mm
$b_{act} = 9.25$ mm
$b_{pass} = (13.25\text{-}2_e)$ mm
R (%)
e (mm)
0
1
2
3
4
5
6
7
8
9
10
2
2.5
3
3.5
4
4.5
5

FIGURE 15

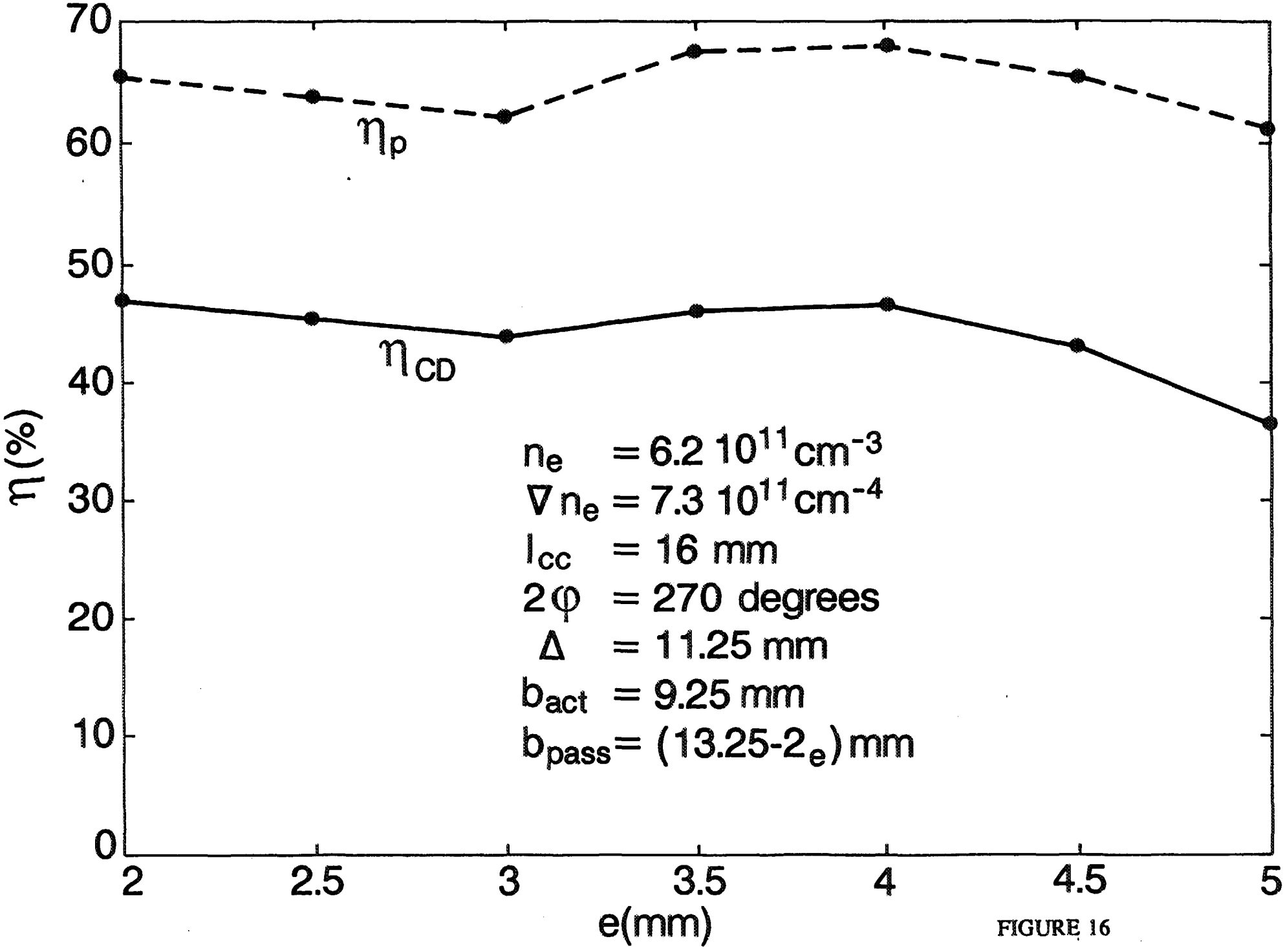
70
60
50
40
30
20
10
0
η(%)
2
2.5
3
3.5
4
4.5
5
e(mm)
η_p
η_{CD}
$n_e = 6.2\ 10^{11} cm^{-3}$
$\nabla n_e = 7.3\ 10^{11} cm^{-4}$
$l_{cc} = 16$ mm
$2\varphi = 270$ degrees
$\Delta = 11.25$ mm
$b_{act} = 9.25$ mm
$b_{pass} = (13.25\text{-}2_e)$ mm

FIGURE 16

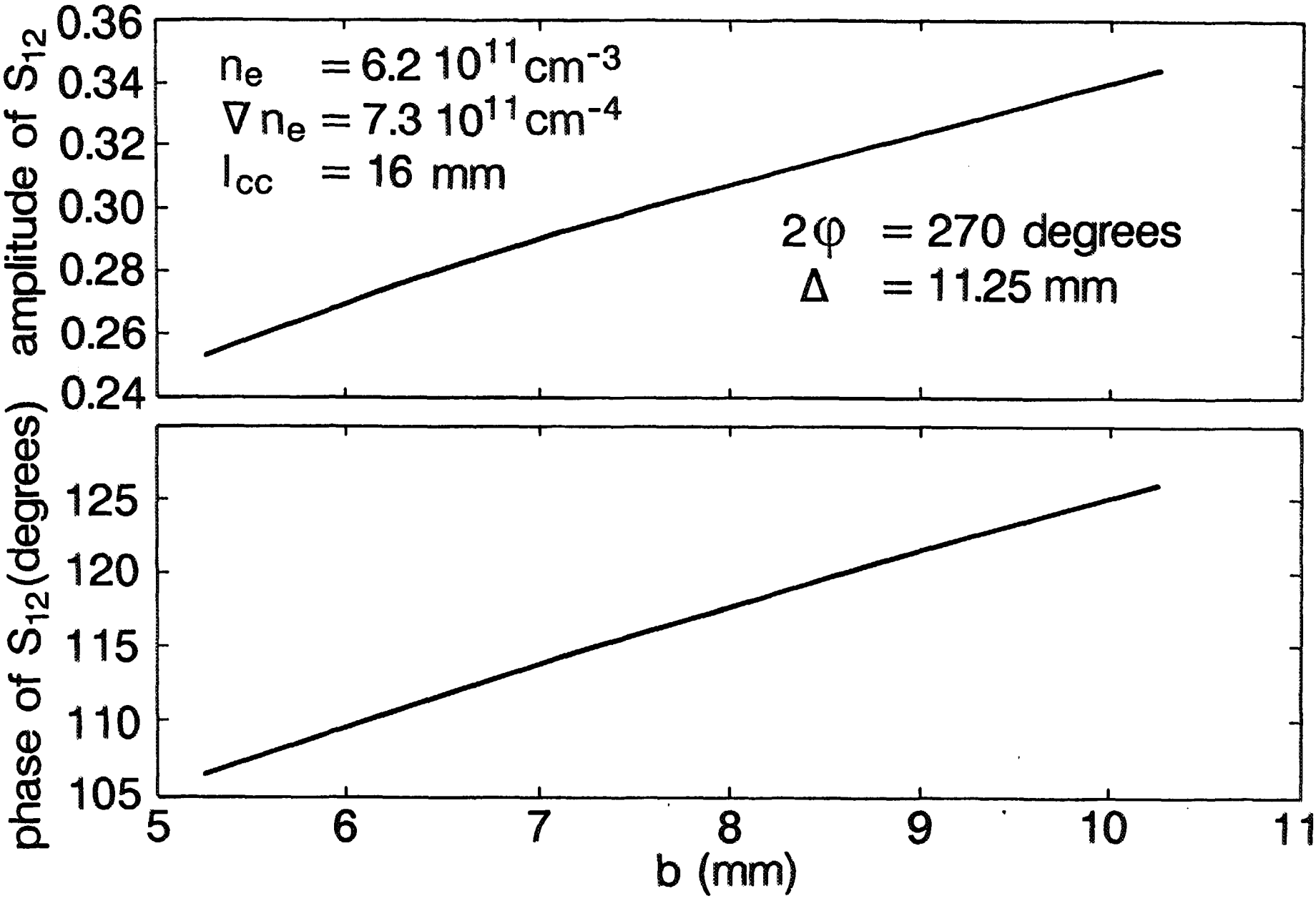
amplitude of S_{12}
0.36
0.34
0.32
0.30
0.28
0.26
0.24
$n_e = 6.2\ 10^{11} cm^{-3}$
$\nabla n_e = 7.3\ 10^{11} cm^{-4}$
$l_{cc} = 16$ mm
$2\varphi = 270$ degrees
$\Delta = 11.25$ mm
phase of S_{12} (degrees)
125
120
115
110
105
5
6
7
8
9
10
11
b (mm)

FIGURE 17

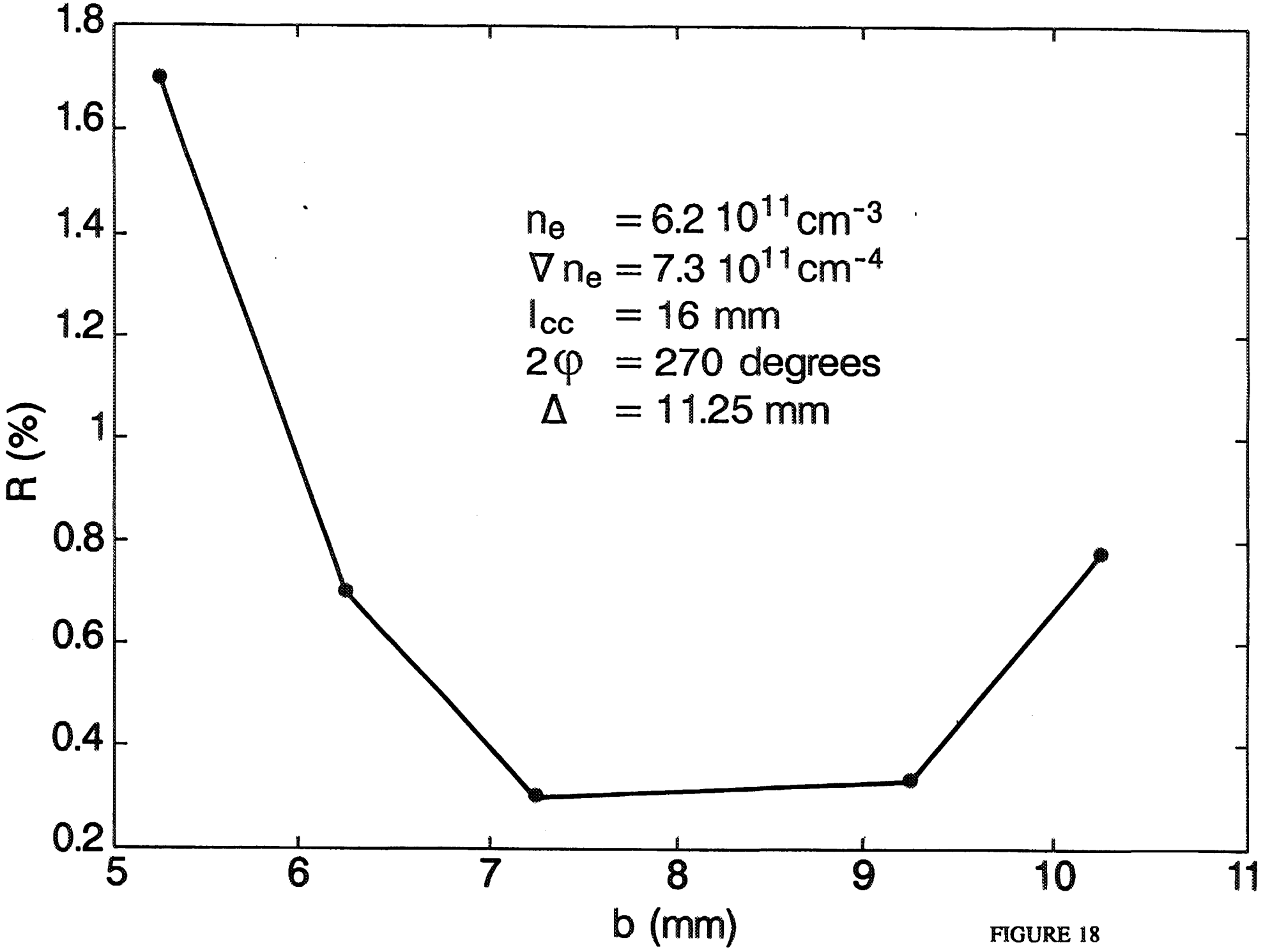
1.8
1.6
1.4
1.2
1
0.8
0.6
0.4
0.2
R (%)
5
6
7
8
9
10
11
b (mm)
$n_e = 6.2\ 10^{11}\ cm^{-3}$
$\nabla n_e = 7.3\ 10^{11}\ cm^{-4}$
$l_{cc} = 16$ mm
$2\varphi = 270$ degrees
$\Delta = 11.25$ mm

FIGURE 18

FIGURE 19

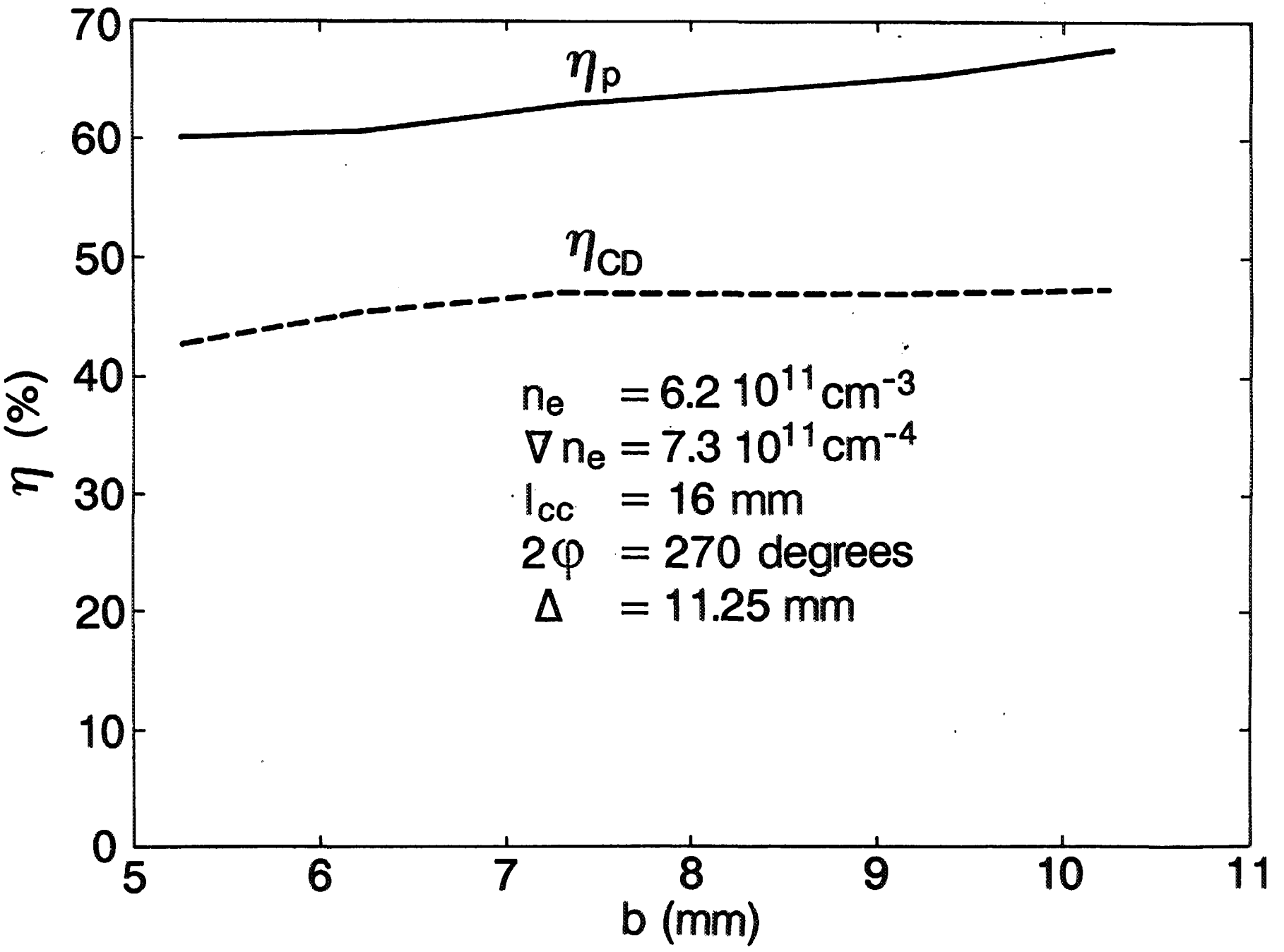
70
60
50
40
30
20
10
0
5
6
7
8
9
10
11
η (%)
b (mm)
ηp
ηCD
ne = 6.2 10^11 cm^-3
∇ne = 7.3 10^11 cm^-4
lcc = 16 mm
2φ = 270 degrees
Δ = 11.25 mm

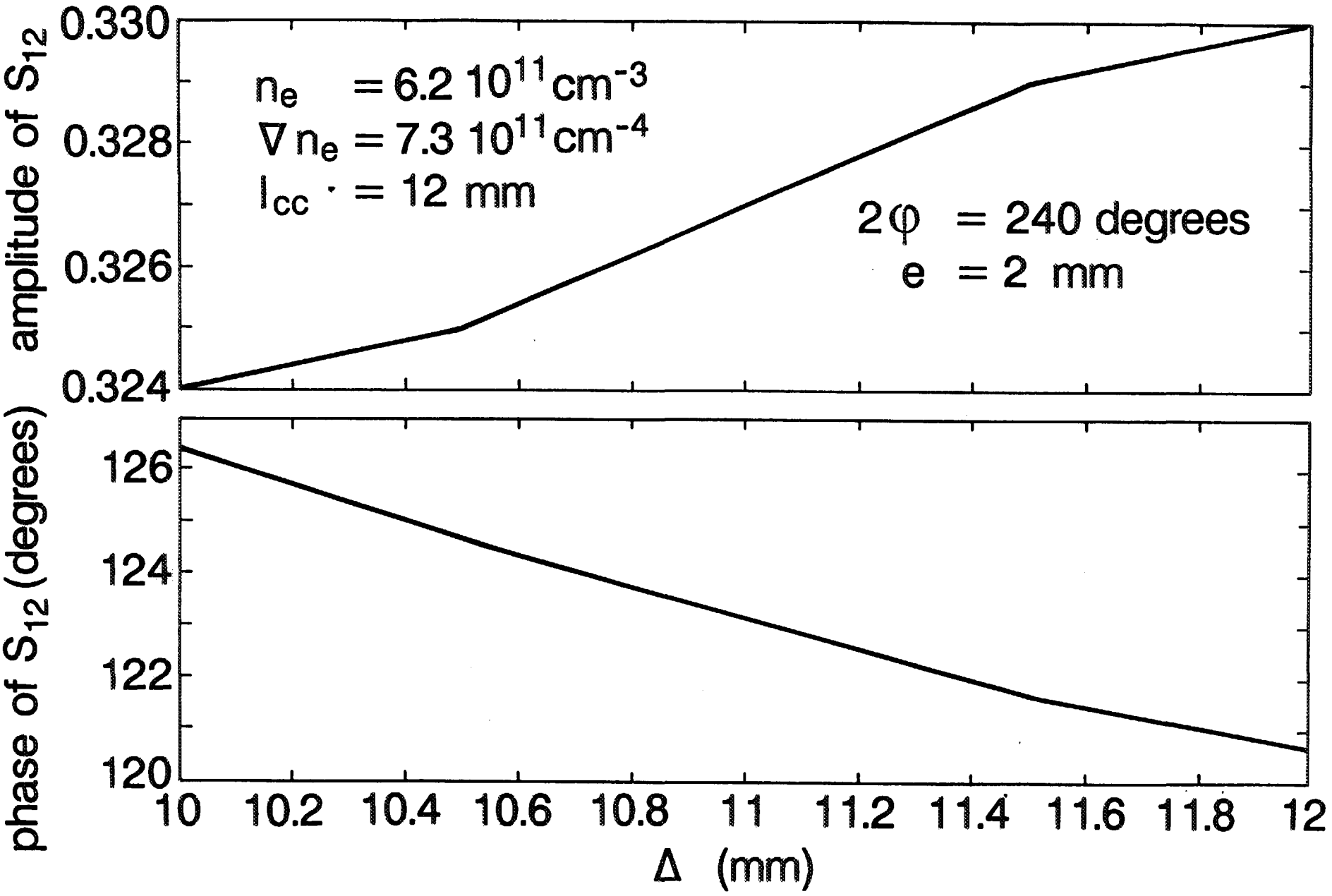
amplitude of S_{12}
0.330
0.328
0.326
0.324
$n_e = 6.2\ 10^{11} cm^{-3}$
$\nabla n_e = 7.3\ 10^{11} cm^{-4}$
$l_{cc'} = 12$ mm
$2\varphi = 240$ degrees
$e = 2$ mm
phase of S_{12} (degrees)
126
124
122
120
10
10.2
10.4
10.6
10.8
11
11.2
11.4
11.6
11.8
12
Δ (mm)

FIGURE 20

FIGURE 21

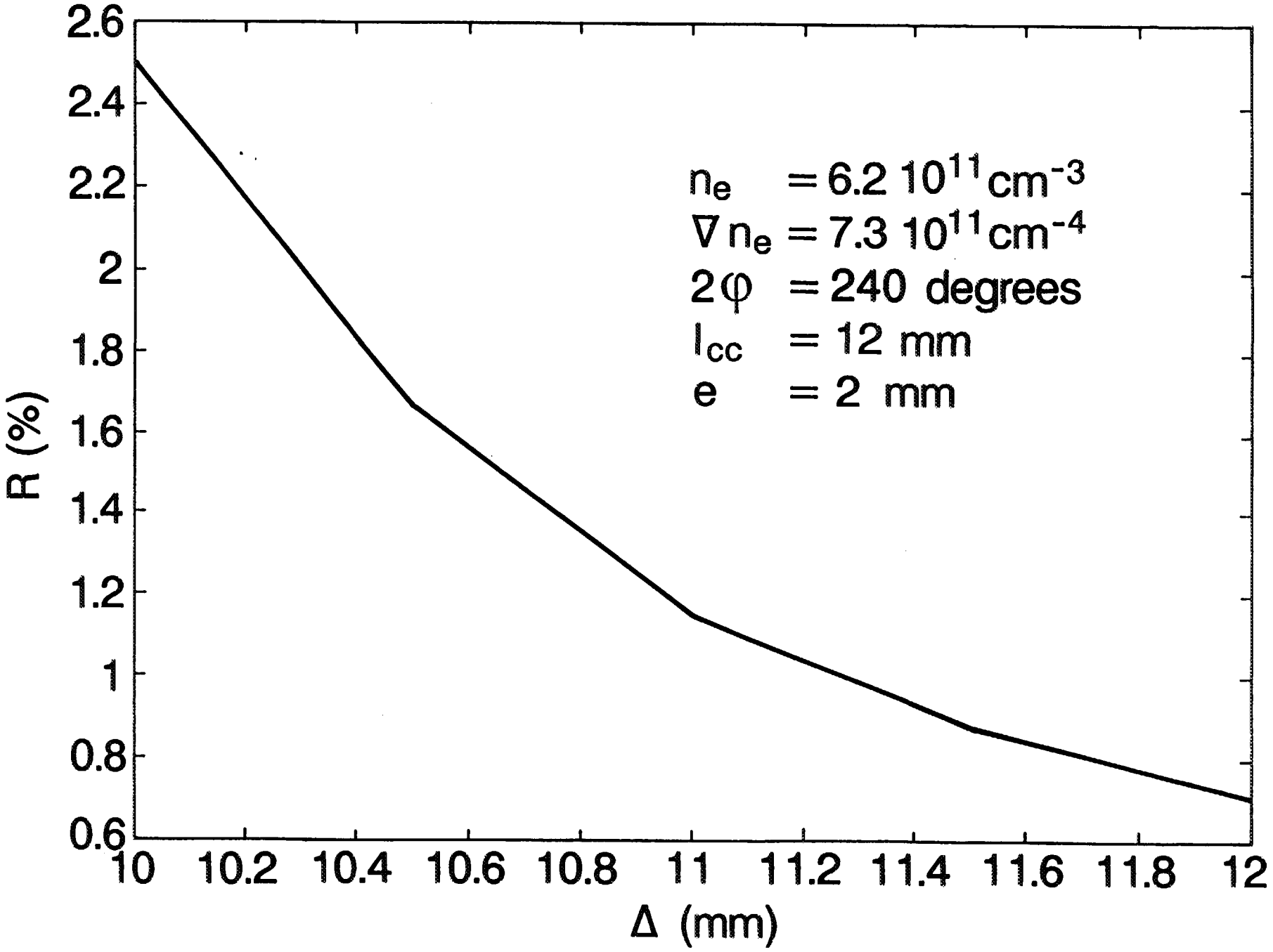
2.6
2.4
2.2
2
1.8
1.6
1.4
1.2
1
0.8
0.6
R (%)
10
10.2
10.4
10.6
10.8
11
11.2
11.4
11.6
11.8
12
Δ (mm)
$n_e = 6.2\ 10^{11} cm^{-3}$
$\nabla n_e = 7.3\ 10^{11} cm^{-4}$
$2\varphi = 240$ degrees
$l_{cc} = 12$ mm
$e = 2$ mm

FIGURE 22

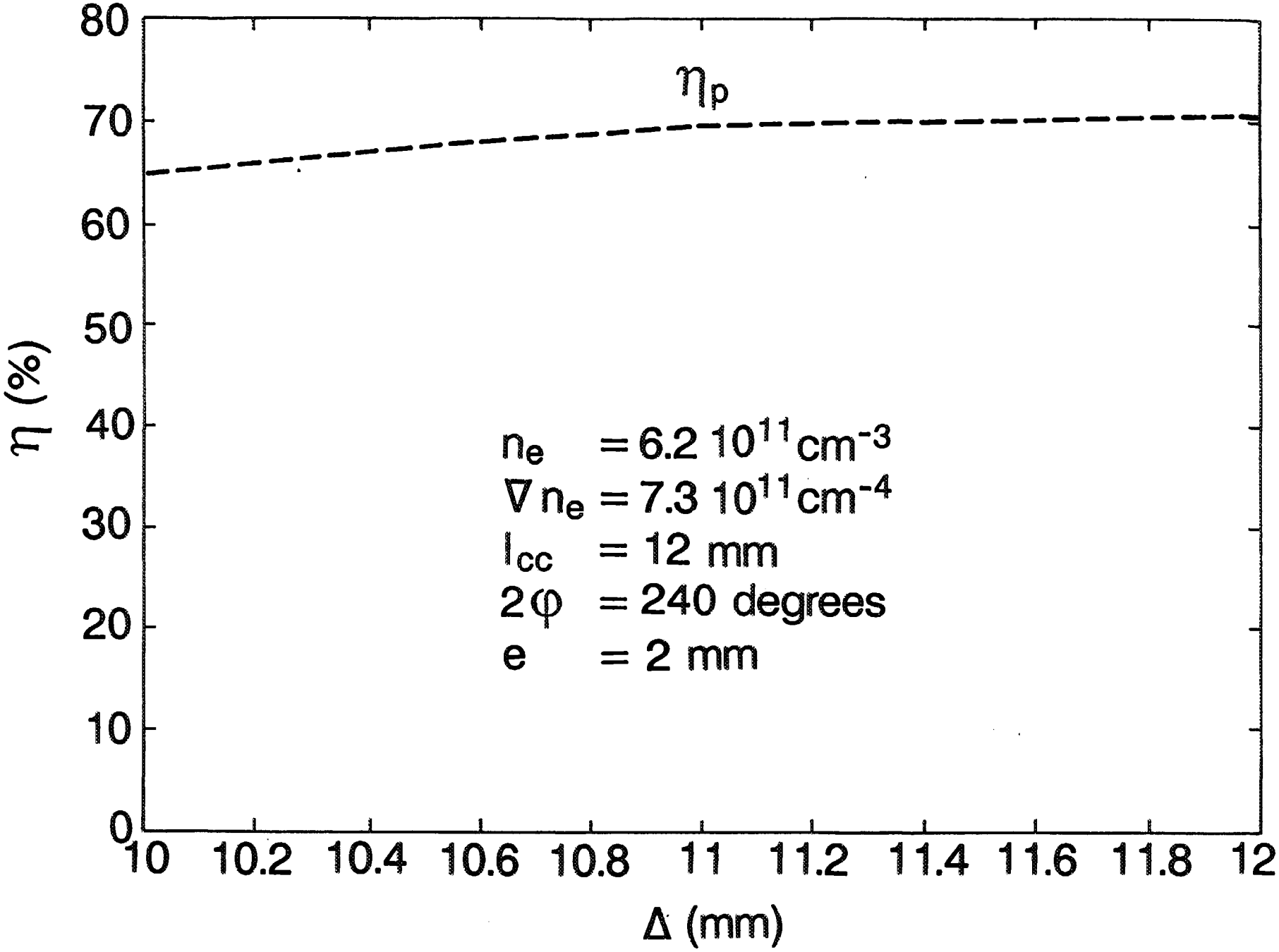
80
70
60
50
40
30
20
10
0
η (%)
ηp
ne = 6.2 10^11 cm^-3
∇ne = 7.3 10^11 cm^-4
lcc = 12 mm
2φ = 240 degrees
e = 2 mm
10
10.2
10.4
10.6
10.8
11
11.2
11.4
11.6
11.8
12
Δ (mm)

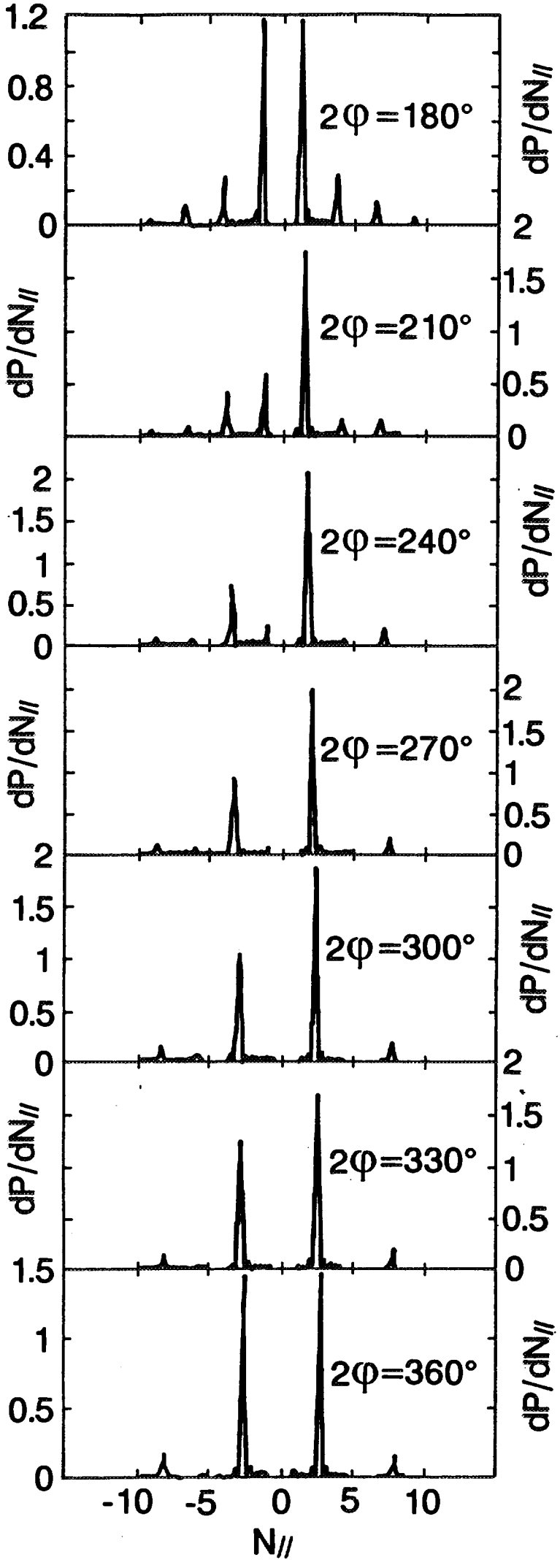

$n_e = 6.2\ 10^{11}\ cm^{-3}$
$\nabla n_e = 7.3\ 10^{11}\ cm^{-4}$
$l_{cc} = 16$ mm
$\Delta = 11.25$ mm

FIGURE 23

FIGURE 24

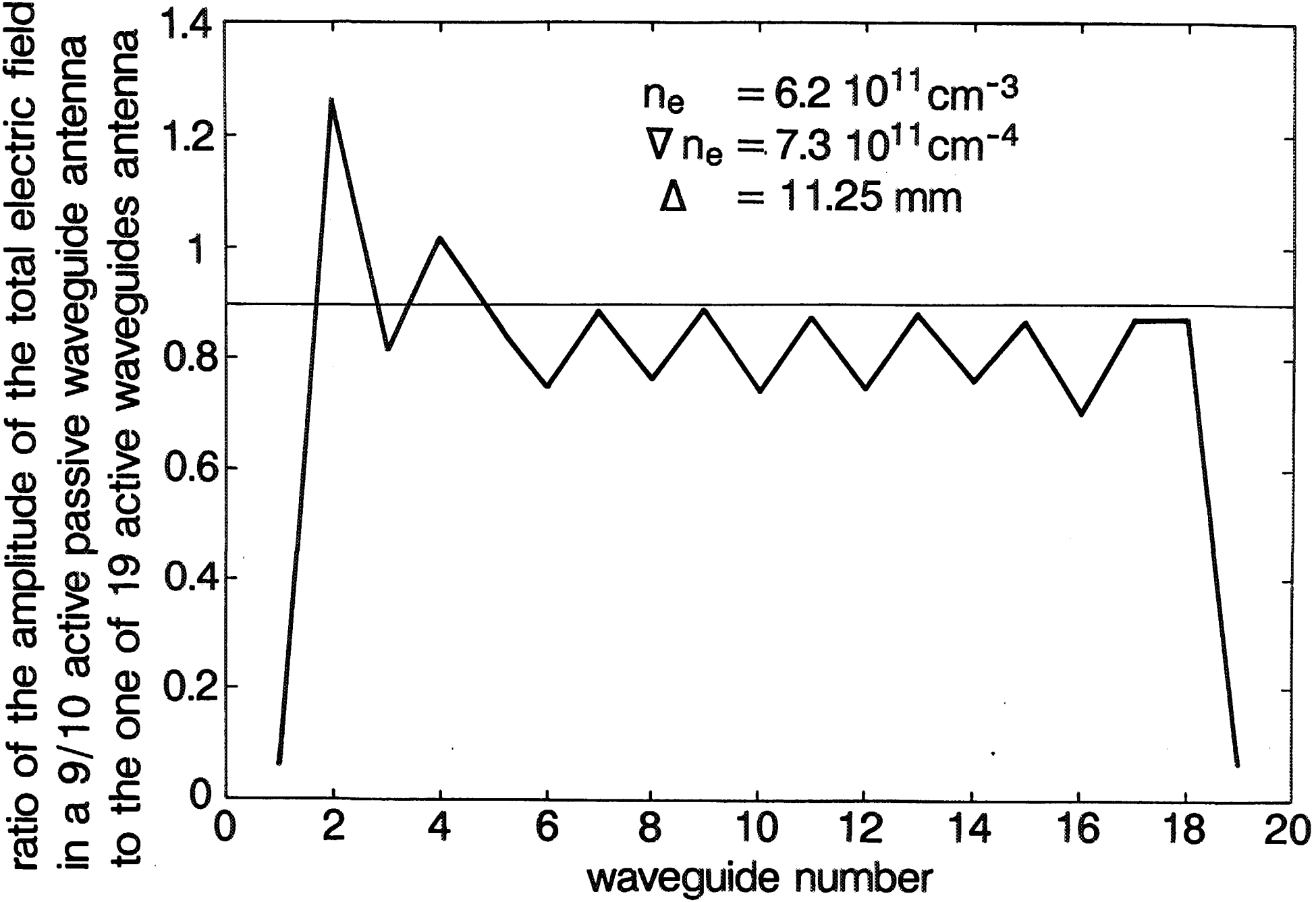
ratio of the amplitude of the total electric field in a 9/10 active passive waveguide antenna to the one of 19 active waveguides antenna
1.4
1.2
1
0.8
0.6
0.4
0.2
0
0
2
4
6
8
10
12
14
16
18
20
waveguide number
$n_e = 6.2\ 10^{11}\,cm^{-3}$
$\nabla n_e = 7.3\ 10^{11}\,cm^{-4}$
$\Delta = 11.25\,mm$